Remote Sensing of Environment 247 (2020) 111807

Contents lists available at ScienceDirect

Remote Sensing of Environment

journal homepage: www.elsevier.com/locate/rse

Coupling high-resolution field monitoring and MODIS for reconstructing wetland historical hydroperiod at a high temporal frequency

Alice Alonso[a,c], Rafael Muñoz-Carpena[a,*], David Kaplan[b]

[a] Agricultural and Biological Engineering Department, University of Florida, 287 Frazier Rogers Hall, P.O. Box 110570, Gainesville, FL 32611-0570, USA
[b] Engineering School of Sustainable Infrastructure & Environment, University of Florida, 102 Phelps Lab, PO Box 116350, Gainesville, FL 32611-6350, USA
[c] Earth and Life Institute – Environmental Sciences, Université catholique de Louvain, Croix du Sud 2, bte L7.05.02., 1348 Louvain-la-Neuve, Belgium

ARTICLE INFO

Edited by Jing M. Chen

Keywords:
Remote sensing
MODIS
Spectral index
Google Earth Engine
Groundtruthing
Wetland
Tropical wetland
Hydroperiod
Hydrology
Flood
Costa Rica
Palo Verde National Park

ABSTRACT

Historical wetland hydrology data are instrumental to support the design of wetland management and restoration strategies but are rarely available. In this study, we tested the capabilities and limitations of a simple methodological framework based on publicly available MODIS Land Reflectance Products to estimate wetland soil surface saturation and inundation spatiotemporal dynamics. Using supervised learning and high-resolution groundwater and surface water elevation data, the framework searches for spectral algorithms, referred to as the wet/dry wetland status classifier (WSC) and the continuous wetland dynamics identifier (WDI), that best predict upper soil layer wetness status in the study wetland. We used Google Earth Engine (GEE) for fast access and processing of the full range of MODIS data. The capabilities of GEE also enabled us to readily conduct a comparative assessment of the MODIS 8-day composite and daily collections and test various pixel-level quality filters to select reliable data at the highest possible temporal resolution. We tested the framework on the internationally-recognized Ramsar site Palo Verde National Park wetland in Costa Rica, and we obtained good results (overall prediction accuracy of 86.6% and kappa coefficient of 0.7 for the WSC; r^2 of 0.71 for the WDI). High-resolution water level data allowed us to assess the challenges, promises and limitations of using MODIS products for wetland hydrology applications. We then applied the WSC and WDI to map the 2000-2016 sub-weekly wetland hydroperiod at 500m resolution, achieving a temporal resolution rarely matched in remote sensing for wetland studies. The analysis of the end-products, combined with the field water elevation data, provided new insights into the drivers controlling the spatiotemporal dynamics of hydroperiod within the Palo Verde wetland and did not reveal any significant temporal trends. The WSC and WDI framework developed here can be useful for reconstructing long-term hydroperiod variability and uncovering its drivers for other wetland systems globally.

1. Introduction

The extent and ecological integrity of wetland ecosystems are facing a rapid global decline caused by water management, pollution, invasive plant encroachment, fragmentation and conversion to alternative land uses (Dixon et al., 2016; Junk et al., 2013). This continuing loss and degradation impairs the numerous ecosystem services that wetlands provide at regional and global scales, including habitat and biodiversity support, carbon sequestration and climate mitigation, water treatment and flood protection, and cultural services (Mitsch and Gosselink, 2007; Zedler and Kercher, 2005). Costanza et al. (2014) estimated that the global annual decrease in wetland area led to global net ecosystem service losses of 9.9 trillion 2007 US dollars per year. Exacerbating these losses are the challenges linked to the restoration and management of wetland ecosystems due to an often-incomplete understanding of long-term wetland degradation drivers and trajectories (White and Kaplan, 2017).

The primary determinant of wetland ecological composition and ecosystem services is wetland hydrology (Mitsch and Gosselink, 2007). Hydrological inputs and outputs influence soil biochemistry, and characteristics of flooding such as duration, spatial extent, and timing of high and low waters drive plants' germination and growth and support the wildlife that depends on this habitat. Hence, by changing physicochemical properties, small changes in wetland hydroperiod – defined here as “the periodic or regular occurrence of flooding and/or saturated soil condition” (Marble, 1992) – can result in significant biotic changes (Boers et al., 2008; Campbell et al., 2016; Mitsch et al., 2010; Osland et al., 2011; Richter et al., 1996; Zedler and Kercher,

* Corresponding author at: University of Florida, 287 Frazier Rogers Hall, P.O. Box 110570, Gainesville, FL 32611-0570, USA.
E-mail address: carpena@ufl.edu (R. Muñoz-Carpena).

https://doi.org/10.1016/j.rse.2020.111807
Received 15 November 2017; Received in revised form 8 March 2020; Accepted 30 March 2020

Table 1
Summary of the key studies that looked at the spatiotemporal dynamics of terrestrial water bodies and wetland hydrology.

Studies that looked at temporal dynamics of the terrestrial water bodies and wetland hydrology					
Study	Satellite data sources	Spatial extent/study case	(i) Method; and (ii) training and validation data sources	Temporal extent and frequency; Spatial resolution	Final products and other key features related with the objectives of our study
Papa et al., 2010	Multi satellite dataset (SSM/I, ERS, AVHRR)	Global	(i) General algorithm combining the three data sources; (ii) Variables such as river discharges and river water level heights.	- 1993 - 2004 - Monthly - 25 km	- Monthly distribution of surface water extent and its variations (GIEMS product); Available upon request; - Captures temporal dynamics even when prevalent cloud cover; - Not suited for smaller-scale wetlands.
Aires et al., 2017	Multi satellite dataset	Global	(i) Downscaled GIEMS 25 km using topography and hydrography information; (ii) Regional wetland cover maps and independant satellite observations.	- 1993 - 2007 - Monthly - 90 m	- Global inundation extent map (GIEMS-D3), ready to use; - Use topographic data for downscaling, which implies lower spatial accuracy as compared to observations from optical sensors (Aires et al. 2018).
Brisco et al., 2017; Hess, 2003; Jaramillo et al., 2018; Kim et al., 2017; Lee et al., 2015; Wdowinski et al., 2008; Wilusz et al., 2017; Yuan et al., 2017; Zhao et al., 2014; Pope et al., 1997	Various SAR	Various: From < 1 km^2 to $> 35{,}000$ km^2	(i) Various i.a. Interferometry SAR; Multivariate linear regression model; Treshold classification; (ii) Various, i.a. Aerial photography; Independent satellites such as GRACE and Landsat; LIDAR; Soil Moisture Active Passive (SMAP) data; Field visits; Groundwater level data; Evapotranspiration estimates.	- From 1 to 9 years between 1993 and 2013 - Two to 15 images per year - From < 100 m to 1 km	- Various products about absolute and relative surface water level and related variables; - Showed that SAR and InSAR can be used to monitor soil moisture content and water level changes; - Can detect water beneath clouds and dense vegetation; - Restrictive data access policies, processing often strenuous, and outputs difficult to interpret; - Lack of regular and long-term temporal coverage.
Yamazaki et al., 2015;	Landsat	Global	(i) Multi-temporal analysis using a general algorithm based on NDWI and a correction factor based on NDVI; (ii) Existing water-body database.	- Multi-temporal analysis from 4 epoch. One final map - 90 m	- Permanent and temporary water bodies map (G3WBM); - Can detect small open water bodies; - Provides incomplete representation of seasonal and smaller-scale wetlands (Aires et al., 2018).
Pekel et al., 2016	Landsat	Global	(i) Expert systems, visual analytics, and evidential reasoning; (ii) Validation based on over 40,000 Landsat-derived control points.	- 1984 - 2015 - Monthly - 30 m	- Map of surface water and its seasonal and long-term changes; - Freely available and ready to use; - No consistent detection of smaller vegetated wetlands (Aires et al. 2018).
https://floodmap.modaps.eosdis.nasa.gov	Aqua/Terra (MODIS)	Global	(i) Algorithm that uses a ratio of MODIS Band 1 and Band 2, and a threshold on Band 7; (ii) Not specified.	- Near real time - 250 m	- Map of floodwater extent for active floods; - Does not detect water in vegetated wetlands.
Tulbure et al., 2016	Landsat	Murray–Darling Basin, Australia ($> 10^6$ km^2)	(i) Random forest with 13 multispectral indices, slope and hillshade as predictors; (ii) Landsat pixels selected via visual interpretation.	- 1986-2010 - Seasonal - 30 m	- Maps of seasonal and interannual surface water dynamics.
Beeri and Phillips (2007); Gómez-Rodríguez et al. (2010); Halabisky et al. (2016); Huang et al. (2011, 2014); Jones (2015); Niemuth et al. (2010).	Landsat	Various	(i) Various: i.e. simple to complex regression spectral models using set of spectral indices and ancillary data to identify surface water for waterbodies, partial unmixing model, and spectral mixture analysis. (ii) Various: i.a. Imagery with finer spatial resolution; National wetland inventory.	- From 1 to 25 years included between - 1984 to 2011 - Monthly to annual (3 to 230 dates) - ≤ 30 m	- Developed and used models for detection of water surface at pixel or sub-pixel level; - Temporal resolution does not allow capturing fast changing conditions; - Large temporal gaps in areas that suffer from persistent cloud cover.
Ordoyne et al. 2007	Aqua/Terra (MODIS)	Everglades National Park ($> 600{,}000$ ha)	(i) Tested various statistical model with a set of six multispectral indices elevation and tree cover as	- 2004 - 16 days - 1 km	- Maps of water depth and flooding likelihood; - Showed that the dynamic hydrology of large

(*continued on next page*)

Table 1 (*continued*)

Studies that looked at temporal dynamics of the terrestrial water bodies and wetland hydrology

Study	Satellite data sources	Spatial extent/study case	(i) Method; and (ii) training and validation data sources	Temporal extent and frequency; Spatial resolution	Final products and other key features related with the objectives of our study
			predictors; (ii) Daily in situ water level averaged to 16-day periods.		wetlands can be accurately mapped using MODIS data.
Feng et al. (2012)	Aqua/Terra (MODIS)	Poyang lake	(i) Used FAI index with gradient method to separate land and water; (ii) 30 m data by the HJ-1A/1B camera.	- 2000–2010 - Monthly - 250 m	- Demonstrated the unique value of MODIS in studying short and long-term inundation changes for highly dynamic lakes.
Murray-Hudson et al., 2014	Aqua/Terra (MODIS)	Botswana's Okavango delta (> 10^6 ha)	(i) Tested (1) supervised and (2) unsupervised learning on the 7 MODIS spectral bands; (3) Band 5:6 ration and (4) band 1 thresholding; (ii) Landsat classified image and 1 date in situ data.	- 2000–2007 - Monthly - 250 m	- Flood extent maps; - Cost-effective and easily implementable; - Preliminary assumptions about the spectral indices are made.
Li et al., 2018	Aqua/Terra (MODIS)	Spatial extent of 2 Landsat tiles in Spain (> 2.10^6 ha)	(i) Random Forest and Cubist using 18 multispectral indices and topographic data; (ii) Landsat and Google Earth high res. mages.	- 2000–2015 - 16 days - 500 m	- Time series of surface water extent and fraction within 500 m wide MODIS pixels.
This study	Aqua/Terra (MODIS)	Palo Verde National Park wetland (8586 ha)	(i) Classification tree and regression analysis with 45 multispectral indices as predictors; (ii) High resolution (15 min) surface and groundwater elevation data from six water stage monitoring stations.	- 2000–2016 - Daily and monthly - 500 m	- Simple methodological framework that uses and is tested with high temporal resolution water elevation data; - Discusses opportunities and limitations of using the full range of MODIS images with such simple framework; - Explains status diagnostic mismatch when working with multiple sensors; - Exemplifies the use of Google Earth Engine for a fast access and processing of the full range of MODIS data.

2004).

Given its importance, quantifying long-term spatiotemporal hydroperiod variability and changes are fundamentally important for many aspects of wetland management and restoration (Acharya et al., 2017). Such data allow to improve the understanding of wetland functioning, to design and calibrate hydrological models, and to investigate the causes of wetland changes. However, field monitoring networks of large wetlands that provide such data are rare because of the difficulty and prohibitive costs associated with large-scale monitoring of these extensive areas, which are often remote and difficult to access (McCarthy et al., 2001; Spiers et al., 1999).

Satellite remote sensing presents appealing opportunities to overcome this issue of data scarcity for studying wetland spatiotemporal hydrodynamics (Davidson and Finlayson, 2007; Rebelo et al., 2018; Rosenqvist et al., 2007). Table 1 summarizes the key studies that have leveraged remotely-sensed database for that purpose. Passive or active (Synthetic Aperture Radar, SAR) microwave remote sensing data can detect inland surface water, are sensitive to soil moisture, and have canopy penetration capabilities while being able to "see" through clouds, making them suitable for wetland monitoring (Henderson & Lewis, 2008; Kasischke et al., 1997; Rosenqvist et al., 2007; Tsyganskaya et al., 2018). For these reasons, these data have been broadly used for mapping wetland inundation and studying wetland hydrology at global (Aires et al., 2017; Papa et al., 2010) and local scales (e.g., Brisco et al., 2017; Hess, 2003; Jaramillo et al., 2018; Kim et al., 2017; Lee et al., 2015; Wilusz et al., 2017; Yuan et al., 2017; Zhao et al., 2014). However, the limitations of radar data lie in the lack of regular and long-term temporal coverage. Additionally, these data can be difficult to access, proces, and interpret (Tsyganskaya et al., 2018). These technical difficulties hinder their routine integration in studies supporting wetland management and restoration.

Multi-temporal and multi-spectral optical remote sensing databases such as the publicly available Landsat products (https://landsat.gsfc.nasa.gov) and the Moderate Resolution Imaging Spectroradiometer (MODIS) Land Data (Justice and Townshend, 2002) offer long-term databases that are easier to access and process. Inland surface water detection with optical remote sensing is relativley simple due to the strong absorbance of the near-infrared (NIR) spectral region, while almost all other land surface types have a high reflectance. A growing number of products of regional to global water bodies at high spatial and/or temporal resolution have been generated using water detection algorithms that build on that property. Landsat imagery have been recently used to produce global maps of permanent and temporary water bodies (Yamazaki et al., 2015) and to produce datasets documenting long-term changes of surface water location and seasonality at a 30-m resolution globally (Pekel et al., 2016) and regionally (Tulbure et al., 2016). Imagery from MODIS has also been used to create a global map of surface water at 250 m resolution (Carroll et al., 2009) and to derive near-real-time global flood mapping at approximately 250 m resolution (https://floodmap.modaps.eosdis.nasa.gov). These remarkable regional to global products offer valuable information to locate open water bodies, track their spatiotemporal variability, and monitor floods. However, wetlands are often covered by floating or emergent vegetation, or populated by trees. As a result, vegetation interferes with the signal reflected by water, and wetland hydric status cannot be reliably detected by algorithms developed for open water detection purposes (Rebelo et al., 2018). Although the "one algorithm for all" cannot be reliably used to track the spatiotemporal variability of vegetated wetlands, several studies have successfully used optical remote sensing to generate information about different aspects of wetland hydrology on a more localized scale.

We identified three standing weaknesses in wetland remote sensing studies. The first is that few studies have proposed a systematic procedure for wetland status identifier exploring a broad range of spectral indices. Nonetheless, a large array of multispectral algorithms have been documented for wetland detection (Benger, 2007; Collins et al., 2014; Domenikiotis et al., 2003; Huang et al., 2014; Landmann et al., 2002; Lee et al., 2007; Li et al., 2015; Lunetta et al., 2006; McCarthy et al., 2001; McFeeters, 1996; Møller-Jensen and Yankson, 1994; Murray-Hudson et al., 2014; Ordoyne and Friedl, 2008; Xiao et al., 2005a; Xu, 2006; Zhang et al., 2014; Zhou et al., 2016). This multiplicity of algorithms reflects the bio-physical diversity characteristic of wetland ecosystems and suggests that appropriate spectral band(s) and their transformation are dependent on the specificities of each wetland system.

The second weakness is that most wetland studies have used training and validation datasets generated from independent aerial or satellite imagery, but few have contrasted results with high resolution in situ data for the scrutiny of the sensitivity and limitations of the remotely sensed diagnostic.

The third is that wetland studies often fail to capture the long-term and rapidly changing processes or abrupt events such as flash floods (Xiao et al., 2004). Although Landsat has been successfully used in numerous instances to scrutinize wetland extent hydrodynamics given its long-term coverage (1984 to present) and fine spatial resolution (30 m) (Gómez-Rodríguez et al., 2010; Halabisky et al., 2016; Huang et al., 2014; Huang et al., 2011; Jones, 2015; Niemuth et al., 2010), its lower revisit frequency impedes the production of a cloud-free dataset of sufficient temporal resolution to capture sub-seasonal dynamics in often-overcast area (Alonso et al., 2016). The daily resolution of the MODIS imagery makes it a particularly good candidate and has been proven well suited for wetland hydrodynamics studies (Feng et al., 2012; Ordoyne and Friedl, 2008) in spite of its coarser spatial resolution (250 m to 1 km). However, most Landsat and MODIS-based studies have looked at temporal changes based on a limited set of "before-after" images, or satellites products at weekly, 16-day, or coarser time resolution (Chandrasekar et al., 2010; Gómez-Rodríguez et al., 2010; Halabisky et al., 2016; Li et al., 2015; Niemuth et al., 2010; Ordoyne and Friedl, 2008). The widespread use of a subset of these databases has been persisting due to the effort required to access and process the multi-temporal archive. Nowadays, powerful computing platforms such as the cloud-based Google Earth Engine (GEE, Gorelick et al., 2017) allow overcoming this barrier by facilitating access to the full depth of optical remote sensing archive and allow for rapid execution of geospatial analyses over the full range of MODIS images. A growing number of studies have leveraged such a platform to untap this spatiotemporal information mine (Alonso et al., 2016; Huang et al., 2017; Midekisa et al., 2017), but the applications for wetland hydrology studies remain scarce.

To address these weaknesses, the objectives of the work were:

(i) to propose and test a cost-effective methodological framework for a site-specific wetland surface status identifier combining the full range of MODIS imagery and high resolution and precision water elevation data;
(ii) to use the framework to reconstruct spatially-explicit hydroperiod history at a high temporal frequency;
(iii) to identify mechanisms underlying the observed variability in long-term wetland hydroperiod.

Our methodological framework involves a classification tree and a regression analysis with an extended list of MODIS spectral indices as input data, and high resolution surface and groundwater elevation data as predictors. It searches for the algorithms that perform best in identifying (i) the upper soil layer wet/dry status, and (ii) the upper soil layer hydric status variability. We referred to the obtained algorithms as the wet/dry wetland status classifier (WSC) and the continuous wetness dynamics identifier (WDI), respectively. Our study site was the 8586 ha Palo Verde National Park (Palo Verde) wetland complex, located in the dry tropics of Costa Rica. Over the past 30 years, the wetland's functions have been altered with a severe vegetation shift. Critical to these ecological changes are expected (but undocumented)

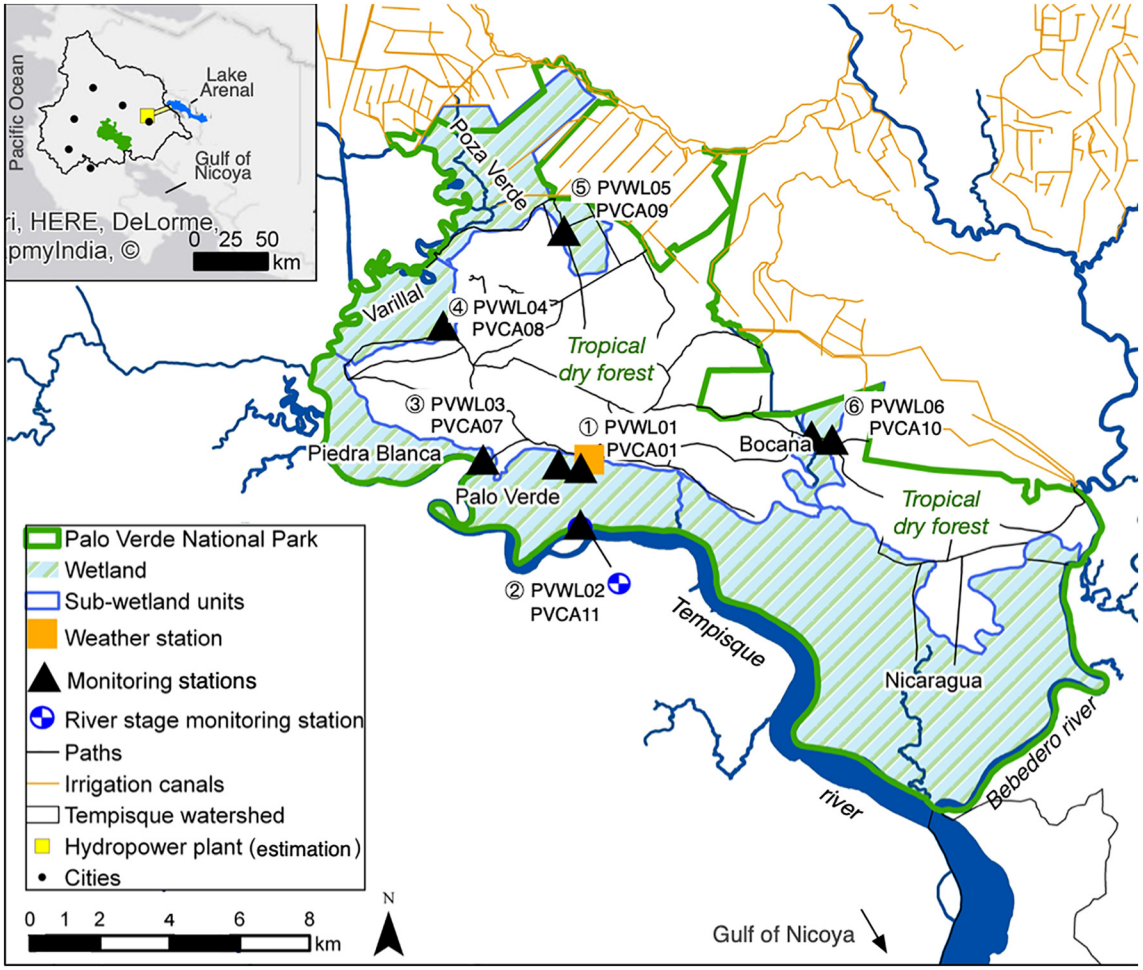

Fig. 1. Palo Verde National Park and wetland and locations of the field monitoring stations. The frame box on the upper left localize the PVNP in the context of the Tempisque watershed (black boundaries).

changes in the magnitude, timing, and spatial extent of wetland inundation.

2. Study site

Palo Verde National Park wetland in the dry tropics of Costa Rica (Fig. 1) is an internationally recognized Ramsar Convention site that provides an ideal testbed for our study because it is a seasonal wetland with high intra- and interannual hydrological variability, and it contains a spatially-distributed hydrological monitoring network that allows testing the sensitivity of the method to soil wetness and depth of ponded water. Climate in Palo Verde is characterized by distinct wet and dry seasons (May to November and December to April respectively), and the region is influenced by the El Niño Southern Oscillation (Waylen and Laporte, 1999; Waylen and Harrison, 2005), which leads to strong interannual variations in rainfall; annual rainfall in the Palo Verde averages around 1325 mm, with a standard deviation of 471 mm (www.ots.ac.cr/meteoro/, 2016). The Palo Verde's wetland soils are vertisols, with high clay content exceeding 55% in the first meter depth (Stipo, 2015).

Water of the Palo Verde wetland is predominantly fresh and dictated by seasonal dynamics. Standing water typically starts accumulating at the beginning of the rainy season and reaches depths > 1 m locally, and then slowly draws down during the dry season. However, the wetland's hydrologic regime is spatially variable due to its uneven topography and adjacency to natural and managed water sources; it is located between the Tempisque and Bebedero tidal rivers, a vast irrigated agricultural district, and a tropical dry forest (Fig. 1), all of which likely contribute water to the system and influence its hydroperiod.

In spite of its RAMSAR status, the wetland is witnessing the encroachment of cattail (*Typha domingensis*), Palo Verde trees (*Parkinsonia aculeata*), and zarza-bush (*Mimosa pigra*), and the subsequent loss of biodiversity and open water bodies needed by waterfowl (Sasa et al., 2015; Trama et al., 2009). Palo Verde is in the outlet of the Tempisque watershed (insert in Fig. 1). The watershed has been significantly transformed since the late 1970s with the implementation of an inter-basin water transfer and damming project designed to support hydropower generation, agricultural irrigation, and tourism development (Edelman, 1987; Jiménez et al., 2001). The downstream location of the wetland makes it vulnerable to these changes, and it is hypothesized that the wetland disturbance today is a consequence. However, there is little understanding of the long-term drivers and mechanisms underlying these wetland changes, which hampers effective management and recovery (Convertino et al., 2016; Jiménez et al., 2001; Murcia et al., 2016).

The Palo Verde wetland is divided into seven units (namely Palo Verde, Chamorro, Piedra Blanca, Varillal, Poza Verde, Bocana and Nicaragua) defined in the Tempisque GIS database procured by the Palo Verde Biological Station, which is managed by the Organization for Tropical Studies (OTS, http://www.ots.ac.cr). Hereafter, we refer to these zones as "sub-wetlands" (Fig. 1). These zones are typically embedded in a natural land depression and filled with water during the rainy season. The sub-wetlands merge into a single body as water

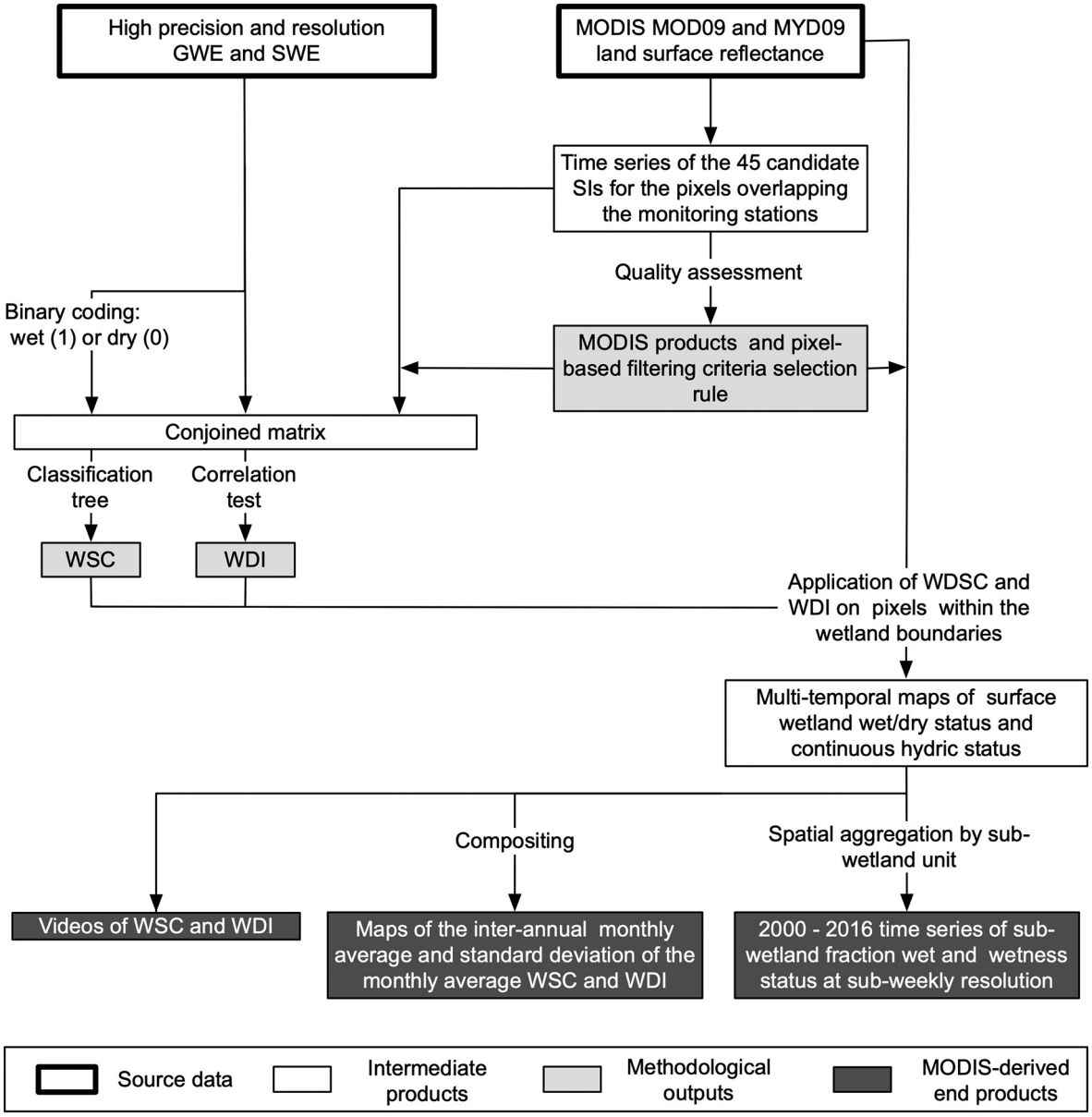

Fig. 2. Methodological flowchart.

accumulates (Dr. E. González, previous Director of OTS-Palo Verde, pers. comm.).

3. Dataset

3.1. Field-measured water elevation

We installed six shallow (2 to 3 m) groundwater elevation (GWE) monitoring wells (Fig. 1) with self-contained pressure transducers (Solinst Leveloggers, Solinst Canada Ltd.) to record water elevation every 15 min from May 2013 to April 2016. For characterizing hydroperiod, we preferred GWE wells over surface water elevation (SWE). Indeed, the groundwater elevation is informative of soil surface wetness since shallow water tables cause the saturation of the upper soil layer through capillarity fringe. However, the first year of data had revealed occurrence of disconnects between groundwater and surface water bodies, so GWE data were insufficient to capture the surface dynamics fully. Therefore, we complemented five of the six GWE wells with co-located surface water elevation (SWE) monitoring wells in May 2014 and April 2015 (Table 1). The SWE wells were instrumented with identical pressure transducer probes or with self-contained canal stage recorders (Schumann and Muñoz-Carpena, 2002). In this paper, the GWE monitoring wells are given an ID starting with PVWL##, and the SWE monitoring wells are given an ID starting with PVCA##. We refer to the paired GWE-SWE wells as "monitoring stations" numbered between 1 and 6 (Table 1). No SWE monitoring well was co-located with the GWE well PVWL01 because there was a SWE well already operating at a nearby location (PVCA01, Fig. 1). We also installed a river stage monitoring station in the Tempisque river. We installed the a monitoring station (monitoring station 2) 100 m inland from that river station to measure the influence of the river on the wetland GWE and SWE (Fig. 1). The locations of the other monitoring stations were chosen to provide relatively even spatial coverage and repurpose an abandoned network of GWE observation wells (PVWL01 and PVWL03 to PVWL06). The locations of these monitoring stations were close to footpaths or service roads, which enabled equipment access and data retrieval. The remote southern portion of the wetland (Nicaragua sub-wetland) was not instrumented in this phase of the project because it was not readily accessible. We used atmospheric pressure data from a barometric pressure sensor (Barologger, Solinst Canada Ltd.) co-located

at the Palo Verde weather station (Fig. 1) to perform barometric compensation of the water level data. Elevation of all repurposed wells except PVWL05 was known from a previous study (JICA, 2002). We surveyed the new wells using the closest repurposed well as vertical datum reference. The elevation of PVWL05 and PVCA09 was estimated as the station was too far from any benchmarks to perform a topographic survey with the material at our disposition. Rainfall data from the Palo Verde weather station were obtained from the OTS online database (OTS, 2016).

3.2. MODIS surface reflectance data

We used MOD09, the 500 m resolution MODIS Surface Reflectance Product holding images corrected for the effects of atmospheric gases, aerosols, and thin cirrus clouds (Vermote et al., 2009). We chose this product because it is freely available, has a sub-daily temporal resolution, and enables water and land cover monitoring through its recording of visible (VIS), near-infrared (NIR), and short wave infrared (SWIR) regions of the electromagnetic spectrum.

MODIS products are recorded by twin sensors aboard the satellites Terra (launched on 12/18/1999 and programmed for a morning overpass time in the Northern hemisphere), and Aqua (launched on the 05/04/2002 and programmed for an afternoon overpass time). The MOD09 product is released in separate datasets for Terra (MOD09) and Aqua (MYD09). In this manuscript, we used the name MCD09 when discussing the combined datasets from Terra and Aqua instruments. We assessed both MCD09 daily and 8-day composite collections (MCD09GA and MCD09A1, respectively). Each pixel in MCD09A1 is made of the best observation within an 8-day period.

We accessed and processed MODIS images with the Google Earth Engine platform.

4. Methods

4.1. Framework for wetland status detection

The methodological flowchart is in Fig. 2. Central to the framework are the *wet/dry wetland status classifier* (WSC) and the *continuous wetness dynamic identifier* (WDI): using our field-measured water level data as training variable, we first used supervised learning with a binary classification tree to search for the combination of candidate SIs that best predicted the wet (upper soil layer is saturated or flooded) or dry (upper soil layer is not saturated) status of a pixel. The resulting spectral algorithm is what we called the WSC. As a complementary approach to the WSC, we assessed whether the time series of any candidate SI could be indicative of the variability of the wetness status, i.e., of the soil moisture content and the height of standing water. The resulting spectral index is what we called the WDI. The framework is detailed in the following sections.

4.1.1. Pixel-based data quality assessment

Data quality assessment at the pixel level is essential for the successful application of MODIS products (NASA LP DAAC, 2014; Vermote et al., 2009). We first verified the quality of each band at the pixel level from the reflectance band quality layer *StateQA* included with the MOD09 product. Secondly, we tested an alternative, less strict filter for removing thick clouds by thresholding the blue band at 0.1 as per Sakamoto et al. (2005). We also tested the effect of excluding pixels with sensor zenith angles > 32.25 degrees to account for possible neighbor effects (Sakamoto et al., 2005). In total, we tested nine combinations of alternative filtering criteria (Table 3). We selected the filtering criteria that secured an acceptable elimination of contaminated pixels while maximizing temporal coverage. We evaluated the filter effectiveness with a visual evaluation of the compactness of the data, and of images before and after the application of the filters.

4.1.2. Candidate spectral indices

We considered the reflectance in the seven MCD09 bands that fall in the visible, NIR, and SWIR spectral regions (bands 1 to 7, Table 4), as well as combinations of these bands, reported in the literature as effective measures for open water or wetland detection. These combinations include variations of a transformed spectral ratio, the normalized difference index (NDI, Eq. (1))

$$\mathrm{NDI} = (\text{band i} - \text{band j})/(\text{band i} + \text{band j}) \quad (1)$$

where the regions of the electromagnetic spectrum measured in bands i and j depend on the application and case study. The MODIS band numbers that we used for the spectral indices (SI) calculation are specified in the SI subscripts (Table 4). We proposed a set of NDIs, building from the two distinct Normalized Difference Water Index (NDWI) equations proposed by McFeeters (1996) and Gao (1996). McFeeters's NDWI was proposed for open water bodies detection and combines the green and NIR bands for R_i and R_j in Eq. (1) respectively, which corresponds to NDI42 following our nomenclature. Gao's (1996) proposed a NDWI for monitoring liquid water content in vegetation canopies and combined NIR and SWIR bands in Eq. (1), which corresponds to NDI25. We tested variations of these two indices by interchanging the NIR and SWIR bands with the three MODIS bands falling in the SWIR range (bands 5 to 7). Testing the sensitivity of these three bands was to account for the property that SWIR can increase contrast between water and other land cover features (Xu, 2006), and that SWIR wavelength interval impacts the NDI sensitivity to other land cover classes in the case of mixed pixels (Ji et al. 2009). Using identical band combinations as for the ones tested for the NDIs, we also defined a set of spectral band ratios (BR) as in Eq. (2)

$$\mathrm{BR_{ij}} = \frac{\mathrm{R_i}}{\mathrm{R_j}} \quad (2)$$

Some studies have shown such SI to perform well (Benger 2007; Collins et al. 2014; Johnston and Barson 1993; Ozesmi and Bauer 2002). We also considered the common vegetation indices NDVI, EVI, soil adjusted vegetation index (SAVI) (Huete 1988), and transformed vegetation index (TVI) as vegetation indices have proven useful for distinguishing water from dry land (McCarthy et al. 2001; Ozesmi and Bauer 2002), and the three Tasseled Cap coefficients (Kauth and Thomas, 1976) that were shown to successfully indicate hydric status in some wetlands (Ordoyne and Friedl 2008). Finally, we also used the so-called “difference in value in EVI and NDWI index” (DVEL), that has been successfully used to detect water in systems where vegetation and water features are mixed, such as estuarine wetlands (Yan et al. 2010) and rice paddy fields (Xiao et al. 2005a). In total, we evaluated 45 SIs (Supplementary Material A – Table A1).

4.1.3. Paired field measurements and MODIS pixels

We paired field-measured water elevation data from each monitoring station with the spectral reflectance values and derived spectral indices extracted from the six MODIS pixels covering their locations (Fig. 3). While the footprint of three pixels was fully encompassed within the wetland, the other three had a minor portion that was not, as reported in Table 2 (Pixel cover) and in Supplementary Material A Figs. A2 to A9. In the case of the monitoring wells PVWL01 and PVCA01, we selected adjacent pixels since the area they covered was more representative of the ground conditions prevailing at the field station (Table 2).

4.1.4. Wetland status classifier (WSC)

4.1.4.1. Training data. We coded the water elevation data as binary values for wet (1) and dry (0) wetland upper soil layer wetness status. We coded wet when the groundwater depth was < 0.2 m (i.e., the water was within 0.2 m from the soil surface). We imposed this below-surface threshold value to account for the capillary fringe that saturates the soil above the groundwater table.

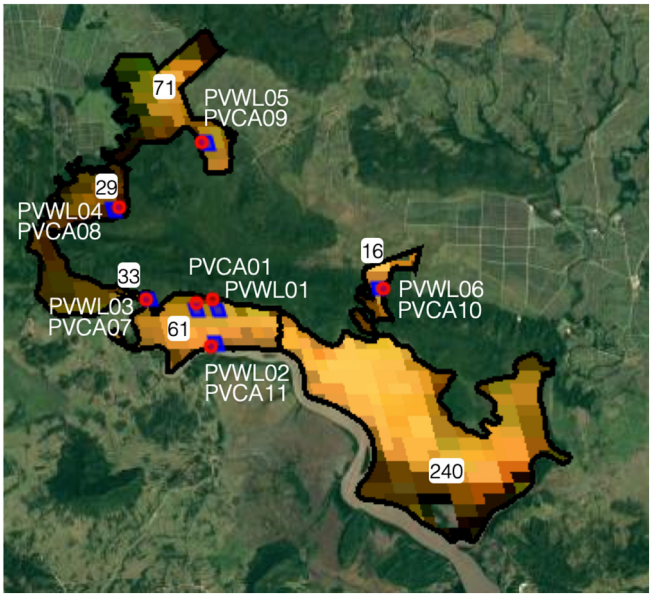

Fig. 3. One MODIS image clipped with Palo Verde wetland boundaries, and location of water level field monitoring stations (red dots) and pixels used for SI calculation (colored in blue). The numbers within the white boxes indicate the number of pixels within the corresponding sub-wetland unit. (For interpretation of the references to color in this figure legend, the reader is referred to the web version of this article.)

4.1.4.2. Classification tree. We trained a classification tree (Breiman et al. 1984) to search for the WSC that best discriminated between the wet and dry status of the wetland using all the candidate SIs as predictors, and the binary-coded field-measured water elevation data as training data. We executed the classification tree with the *fitctree* function (The Mathwork Inc., 2018). In a classification tree, each node holds conditional tests applied to the input variables and splits into branches representing the outcome of the tests. The terminal node holds the class labels (wet or dry) under which the input variables – referred to as *leaves* – are classified (Breiman et al. 1984). To avoid overfitting (i.e. a deep, multi-level tree that has a high prediction accuracy with the training variables but fails when predicting with independent inputs), we controlled the tree depth by imposing a minimum number of leaves per node. We determined that number by testing the prediction performance for an incrementally increasing imposed minimum number of leaves. We selected the highest number that did not involve a significant decrease in performance. For robustness, we assessed each iteration by taking the averaged performance of a series of 10-fold cross-validations consisting of partitioning the training data into ten subsets, nine being used as the training sets and one as the testing set in a recursive manner (Matlab, Statistics and Machine Learning Toolbox. The Mathwork Inc., 2018).

We used water elevation time series data from the monitoring station 1 as a training dataset because surface and groundwater elevations at this site were tightly coupled and thus served as a reliable indicator for wetland surface wetness status.

4.1.4.3. Assessment of the WSC. We tested the robustness of the resulting classification tree (that is, the WSC) by evaluating its classification success rate with the field data measured at stations 2 to 6 within a confusion matrix (Yuan et al. 2017). We used the overall and individual station prediction accuracy percentages as well as Cohen's kappa coefficient that considers random chance. An important aspect that our study took into consideration is that the wetness status diagnosed by the three types of sensors used in this study (MODIS, groundwater elevation, and surface water elevation sensors) can differ depending on the source of water controlling the upper soil layer wetness status, as depicted in Fig. 4. For example, the upper soil layer can be saturated due to the shallow water table capillarity fringe effect that saturates the soil above. In such a case, it should be diagnosed wet by the MODIS sensor, although GWE measures the water elevation below the ground surface (Fig. 4B). A diagnostic mismatch can also occur between these two sensors due to the temporally-lagged response between the groundwater table drawing down and the drying of the soil surface. To overcome the uncertain diagnostic made with GWE data due to these phenomena, we assumed that the wetland was dry when the groundwater depth was > 1.5 m, and wet when it was < 0.2 m with respect to ground surface elevation. Because we do not know the exact height of the capillarity fringe, we excluded data measured at intermediate depths (0.2 to 1.5 m) during the WSC training. We considered the surface wet regardless of the groundwater level when the surface water elevation monitoring wells recorded standing water (Fig. 4D & E). We did not include points for which the dry or wet upper soil layer hydric status could not be ascertained by the field data in the calculation of the prediction accuracy and kappa coefficients.

4.1.5. Wetland continuous wetness dynamics identifier (WDI)

Using Pearson's correlation coefficient, we first selected the spectral index most strongly correlated with groundwater elevation at station 01 (PVWL01). To support a visual evaluation of the index's ability to capture wetness status dynamics, we transformed the final spectral index and water elevation to a common scale using unity-based normalization as in Eqn (3):

$$X_{norm} = \frac{X - X_{0.01}}{X_{0.99} - X_{0.01}} \quad (3)$$

where X is the variable to normalize and $X_{0.01}$ and $X_{0.99}$ are the 1st and 99th percentiles to exclude any extreme values not detected with the pixel-based filtering procedure.

4.2. Reconstruction of hydroperiod history

We applied the selected pixel-level quality filter and the wetland WSC and WDI to all the pixels covering the Palo Verde wetland and the ensemble of images in the MODIS imagery. Then, we generated a suite

Table 2
Ancillary information about the field monitoring stations and the corresponding MODIS pixels.

Field monitoring station no	Latitude (WGS84)	Longitude (WGS84)	Groundwater elevation (GWE)		Surface water elevation (SWE)		Pixel cover (%)
			ID	Date start (MM/DD/YY)	ID	Date start (MM/DD/YY)	
1	10.345	−85.340	PVWL01	05/14/13	PVCA01[a]	05/01/13	100
2	10.326	−85.340	PVWL02	05/13/13	PVCA11	04/25/15	84
3	10.343	−85.366	PVWL03	05/02/13	PVCA07	05/01/14	88
4	10.378	−85.376	PVWL04	05/02/13	PVCA08	05/02/14	100
5	10.402	−85.344	PVWL05	05/02/13	PVCA09	05/03/14	100
6	10.348	−85.275	PVWL06	05/02/13	PVCA10	05/04/14	93

[a] GWE and SWE wells are 700 m apart. Geographic coordinates of the SWE well: (−85.346, 10.342).

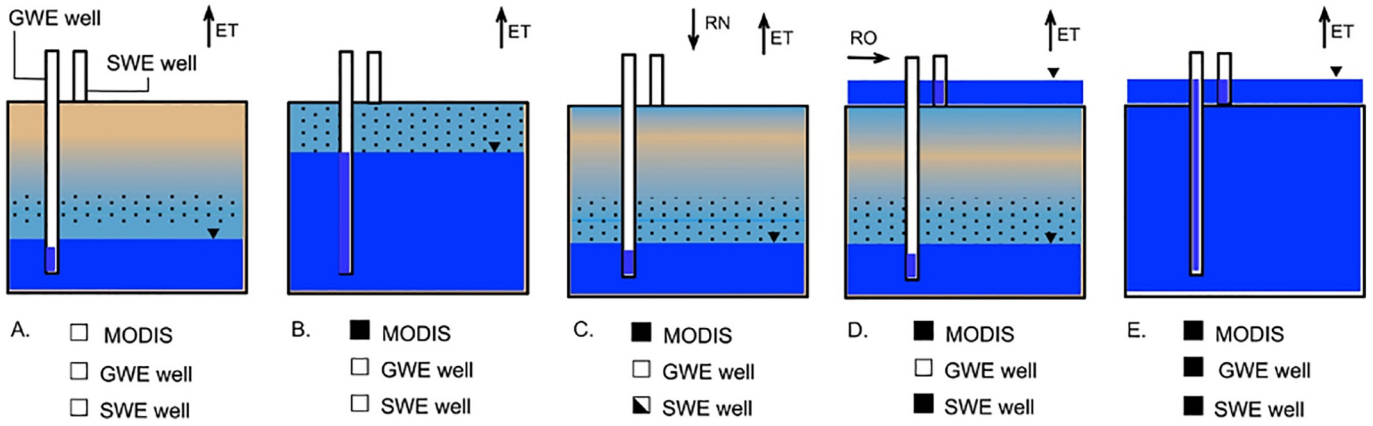

Fig. 4. Seasonal wetland soil column profiles illustrating different phenomena controlling the upper soil layer wetness status and the diagnostic (■: wet; □: dry; ◪: either) made by the three types of sensors, highlighting the cross-sensor agreement or mismatch. Dark blue: aquifer or standing water; water table; dots: capillary fringe; and sky blue to brown: soil of decreasing soil moisture content. RN: rainfall; RO: runoff and/or river bank overflow; ET: evapotranspiration. A) Dry wetland: no water input and the water table or capillary fringe do not reach the upper soil layer. B) Wet wetland with capillary fringe: the capillary fringe saturates the upper soil layer. C) Wet wetland by excess rainfall or runoff: input water intensity exceeds the infiltration rate. It saturates the upper soil layer, although the water table is deep. D) Lateral flooding. E) Saturated soil resulting from the transitioning from (B) or (D) after a sustained input of water, which saturates the entire soil column. Additional water accumulates at the surface. (For interpretation of the references to color in this figure legend, the reader is referred to the web version of this article.)

of MODIS-derived products in the Google Earth Engine (Gorelick et al. 2017) and Matlab (The Mathwork Inc, 2018) to support visualization and analysis of wetland hydroperiod spatiotemporal variability and history. These products include (i) time-lapse videos from April 2013 to March 2015 – two years that witnessed above and below average total annual rainfall – of the MODIS imagery processed with the WSC and WDI; (ii) for each month of the year, maps representing the interannual averages and standard deviations of the frequency at which the pixels were detected wet by the WSC (i.e., the ratio between the number of images in which it was detected wet and the total number of images for that month), and the interannual monthly averages and standard deviations of the WDI; (iii) sub-weekly and monthly-averaged time series of the percentage area of each sub-wetland unit detected wet with the WSC, and of the average and standard deviation of the WDI. Before generating these products, we removed the images when > 10% of the pixels within the Palo Verde wetland area were filtered out by the pixel-level quality filter.

5. Results

5.1. Framework for wetland wetness status detection

5.1.1. Field-measured water elevation time series

Field-measured water elevation time series are displayed in Fig. 5. Detailed analysis is provided in Supplementary Material B. The data showed occurrences when surface water decouples from the shallow groundwater table (indicated as GWE-SWE disconnect in Fig. 5). The prolonged period from May 2013 to January 2014 during which the groundwater elevation at PVWL02 remains below the ground level strongly suggests another case of sustained disconnect between groundwater and surface water. When there is such disconnect, the upper soil layer wetness diagnostic made by GWE sensors is different than by SWE and satellite sensors (Fig. 4 D). This diagnostic mismatch had to be taken into consideration when training and assessing the WSC.

5.1.2. Pixel-based quality filters and assessment of the MODIS products

Figs. 6, 7 and Figs. A11, A12 and A13 in Supplementary Material A are different representations of the values of the spectral indices BR_{26} calculated with the two products MOD09GA and MOD09A1 after the application of the quality filters (Table 3). They reveal that blue band thresholding (filter 4) efficiently filtered out the noise from the signal while eliminating less data than the filters that included MODIS quality flags. In other words, using the single blue band thresholding filter 4 maximizes the data frequency and minimizes the occurrence of long data gaps (Fig. 8).

Fig. 7 shows the effect of different filters on the total number of images. This figure also tests whether the filtered data remain confined within the boundary of the dataset resulting from the most constraining filter 9. Our filter selection is supported by the fact that most of the points of the datasets filtered with filter 4 falls within that envelope. Although adding the sensor zenith angle constraint (filter 6) slightly reduces the apparent noise in the data (Supplementary Material A – Figs. A11 and A12), we considered this improvement to be nullified by the associated decrease in data frequency and temporal continuity.

Figs. 6 and 7 also show that the MYD09 dataset (from Aqua satellite) consistently exhibited higher unstructured variability for the study area (see also Supplementary Material A – Figs. A11, A12). This is likely caused by remnant small clouds or haze undetected by the filters since the overpass time of the Aqua satellite is during the afternoon, when convective atmospheric storms prevail. Consequently, we excluded the MYD09 dataset from the analysis. After the screening procedure was applied, the MOD09GA daily dataset closely matched the 8-day composite MOD09A1 (Fig. 6). Given these outputs, all subsequent analyses were performed using the MOD09GA product screened with filter 4.

5.1.3. Wetland wet/dry status classifier

For the Palo Verde wetland, a classification tree with a single split had equivalent or higher prediction accuracy than a tree with multiple branches. The WSC for Palo Verde wetland was BR26, the ratio between band 6 (SWIR, 1628–1652 μm) and band 2 (NIR, 841–876 μm), with a threshold value of 1.66. In other words, the WSC for Palo Verde classifies as "wet" pixels with BR26 values higher or equal to 1.66.

The water elevation monitored by the field stations color-coded in blue or yellow for wet or dry classification by the WSC is plotted in Fig. 9 and shows good agreement between measured and predicted wetness status. The prediction accuracy and Cohen's kappa coefficients for the training dataset were 91.3% and 0.80 respectively (Table 5). When tested with all the other water level monitoring stations but station 2, the WSC accurately identified 86.6% (78.0 to 90.9%) of the data as wet or dry, with kappa coefficients ranging from 0.5 to 0.8, attesting for a moderate to very good agreement for those stations

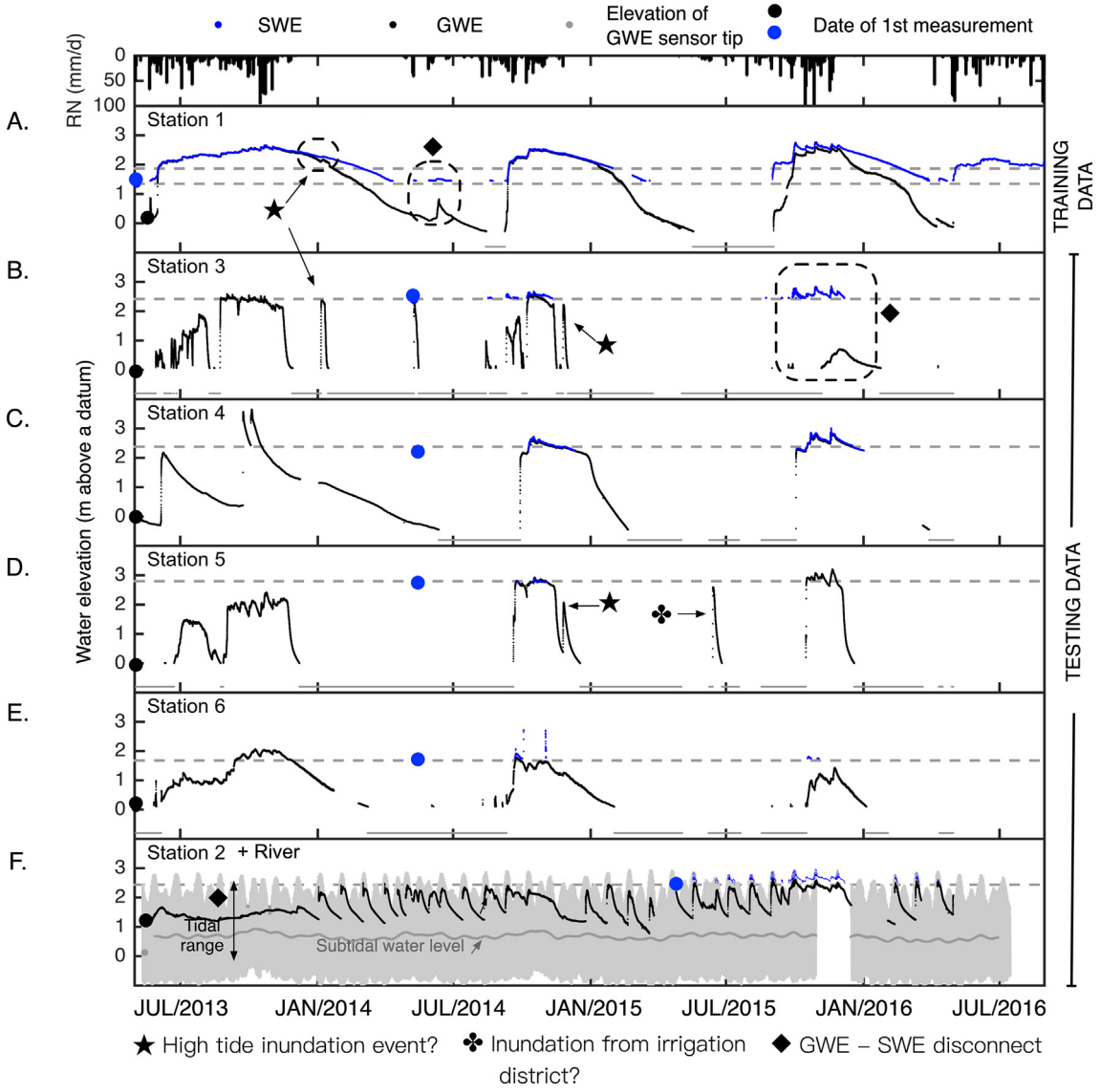

Fig. 5. Rainfall (RN) at the weather station and 15-minute groundwater elevation (GWE) and surface water elevation (SWE) at the field monitoring stations. SWE is only plotted when there is ponding water. Dashed lines indicate ground level for all the stations where SWE and GWE wells are < 1.5 m apart; at station 1, where wells are 700 m apart, one line is provided for each well. Light grey in (F) subplot is the tidally influenced river stage (Fig. 1). Grey dots in the bottom axis of each subplot indicate when the water level fell under the sensors' tips. Data gaps are due to sensor malfunction.

(Table 5 and Fig. 9). The lower performance for station 2 is mostly due to the prediction by WSC that station 2 was wet from 05/2013 to 01/2014, despite the groundwater depth being below 1 m (Fig. 9). This diagnostic mismatch is very likely attributable to a misleading diagnosis about the upper soil moisture status by the GWE sensor during an episode of groundwater – surface water disconnect as explained in Section 5.1. and Fig. 4D. This assumption cannot be verified by field monitored data since we only started measuring surface water elevation at station 2 in May 2015, i.e. after this period occurred.

In some other cases (Stations 3 and 5), the prediction accuracies for the classification is lower for wet than dry cases, i.e. the MODIS product detects more cases of saturated or inundated status than measured by field sensors. This likely results from the diagnostic mismatches illustrated in Fig. 4B to D. For example, the wet status prediction by MODIS during a period of low groundwater level in June 2014 for PVWL01, 03 and 06 (Fig. 9), is likely due to the phenomenon depicted in Fig. 4C: rainfall moistened the wetland surface at the beginning of the rainy season when the aquifer water level was still deep underground. Another example of this is found in Station 3 and 5 during January 2015. There, the water level dropped abruptly, but the upper soil layer remained saturated by capillary fringe or runoff from the nearby river (Fig. 4B and C). Under these assumptions, MODIS rightfully captured the upper soil layer moisture status in both example cases, whereas the GWE and SWE sensors did not. Additionally, the coarse pixel size might play a role in this apparent misclassification as hinted by the measurement of standing water during that time frame at the surface water monitoring well PVCA01, 700 m away from well PVWL01. Therefore, the pixel area likely exhibited standing water at one location, and shallow groundwater at another.

While the WSC at the monitoring station 2 (~100 m from river edge) failed to consistently detect flooding by river overbank flow events (that are indicated by the sudden spikes in groundwater elevation data in Fig. 9), there was a higher frequency of wet status prediction during the dry season, when these events occur (Fig. 9, dashed circles).

5.1.4. Wetland wetness dynamics identifier

BR26 was also the SI with the strongest relationship with measured

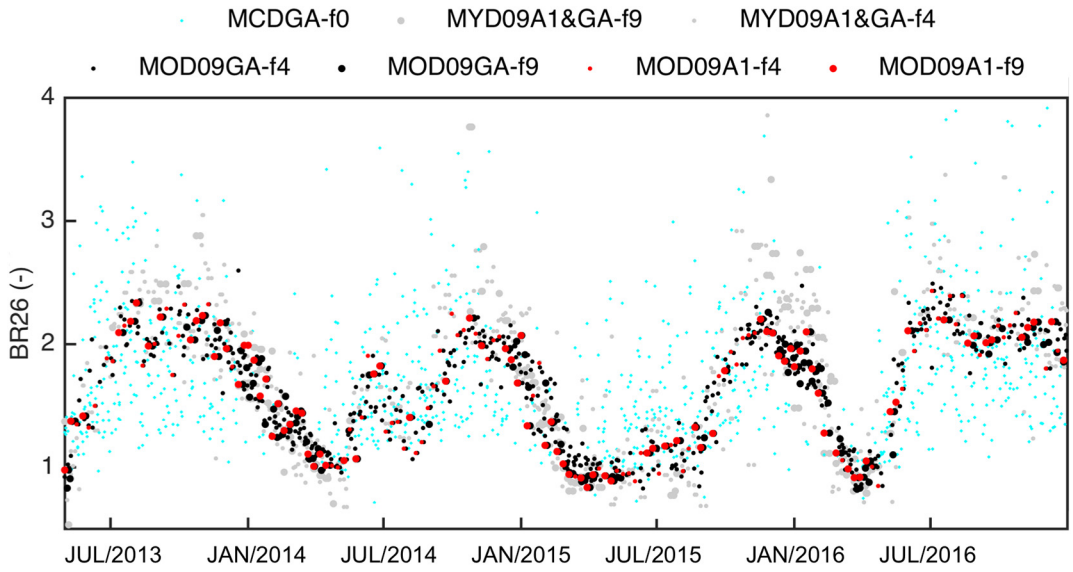

Fig. 6. Time series of BR_{26} from four alternative MODIS sensor sources (Terra – MOD, Aqua – MYD, or both – MCD), collections (daily – 09GA or 8-day composite – 09A1), and filtering criteria (f#).

GWE at monitoring well PVWL01 (R^2 = 0.71 Supplementary Material A – Fig. A14). Fig. 10 shows a similar dynamic between the normalized BR26 and water level at the other monitoring locations, although the water elevation fluctuates more abruptly with sudden rises and falls. We think that this behaviour is due to a sandy layer underlying the clay layer and that acts as a drain, hence rapidly emptying or filling the groundwater storage with water. However, due to the lagged response between the groundwater level and the soil moisture, it is reasonable to think that the upper soil layer wetness follows a smoother pattern that matches with BR_{26} (Fig. 10).

5.2. Reconstruction of hydroperiod history

Raw and monthly-averaged time series data of the fraction of each sub-wetland superficial area detected wet by the WSC are shown in Fig. 11. The spatiotemporal wetting/drying patterns and variability across the wetland from 2000 to 2016 are displayed in the composite maps of interannual, monthly average and standard deviation of the wetness values diagnosed by the WSC and WDI in Fig. 12 and Supplementary Material A – Fig. A16. Daily time step videos of the WSC and WDI values are in Videos 1 and 2. The main expected drivers (landscape features and precipitations) are indicated in the products where and when relevant to support the interpretation of the observed spatiotemporal variability. These time-lapse videos clearly display the wetting and drying patterns in phase with rainfall and reveal that portion of the wetland in the river fringe and in areas adjacent to the irrigation districts become wet during the dry seasons.

6. Discussion

6.1. Framework for wetland status detection

6.1.1. Field-measured water elevation time series

Overall, the field monitoring data (Fig. 5) revealed complex hydrologic patterns within the wetland. They showed that wetland is seasonally flooded, and suggest that surface wetness is largely driven by precipitation and groundwater, river-bank overflow during major spring tide events, and suggest the occurrence of flooding from the irrigation district. When conducting the fieldwork, we also observed (but did not measure) intermittent runoff controlling wetland surface wetness. Although the latter three water sources are not as important in magnitude as precipitation and groundwater, our data showed that they play an important role in controlling the timing and frequency of inundation and hence hydroperiod.

In addition to their use for training the spectral algorithm, the field measurements reveal and measure a high point-scale temporal variability of water elevation that remotely sensed data was not able to capture. Therefore, our study illustrates that in-situ, high-resolution data is complementary to remotely sensed data. Such a hybrid approach should, therefore, be preferred whenever possible. Importantly, these data also helped to identify and describe sensor diagnostic mismatches that needed to be taken into account when conducting our study and could guide others.

6.1.2. Pixel-based quality filter and assessment of the MODIS products

The ease of data access and processing with the cloud-based Google Earth Engine platform allowed us to use the full-depth of the MODIS archive to compare daily productswith 8-day composites. This enabled the observation of the wetness status of the wetland at any specific date in the past, granted that the image was not filtered out.

The selection of the less-constraining filter 4 (blue-band thresholding as per Sakamoto et al. (2005)) allowed us to increase the temporal frequency of the data and reduce the length of the temporal data gaps (Fig. 8 and Supplementary Material A Figs. A11 to A13). Although the filter appeared to perform well for our study case, this might not be the case for other case-study applications. Filter assessment remains a required preliminary step, and the MODIS quality assurance information should be preferred in case for which high temporal resolution data is not required.

The results of this study also highlighted a clear difference in the signal quality from images sensed by sensors mounted in the Terra (AM overpass) and Aqua satellites (PM overpass). The latter showed more unexplained variability – likely caused by undetected haze/storm activity prevailing during the afternoon in this tropical area – and was therefore excluded from this analysis. This important finding should incentivize future studies to systematically assess both datasets individually before deciding on the use of either or both.

6.1.3. Wet/dry WSC and continuous WDI

Our results showed that simple binary (wet/dry WSC) and continuous (WDI) spectral algorithms could capture wetland hydric status and dynamics. WSC and WDI are complementary of each other. The WSC provides a clear wet/dry diagnostic (e.g. to characterize hydroperiod such as in Fig. 11) and WDI tracks continuous inundation or

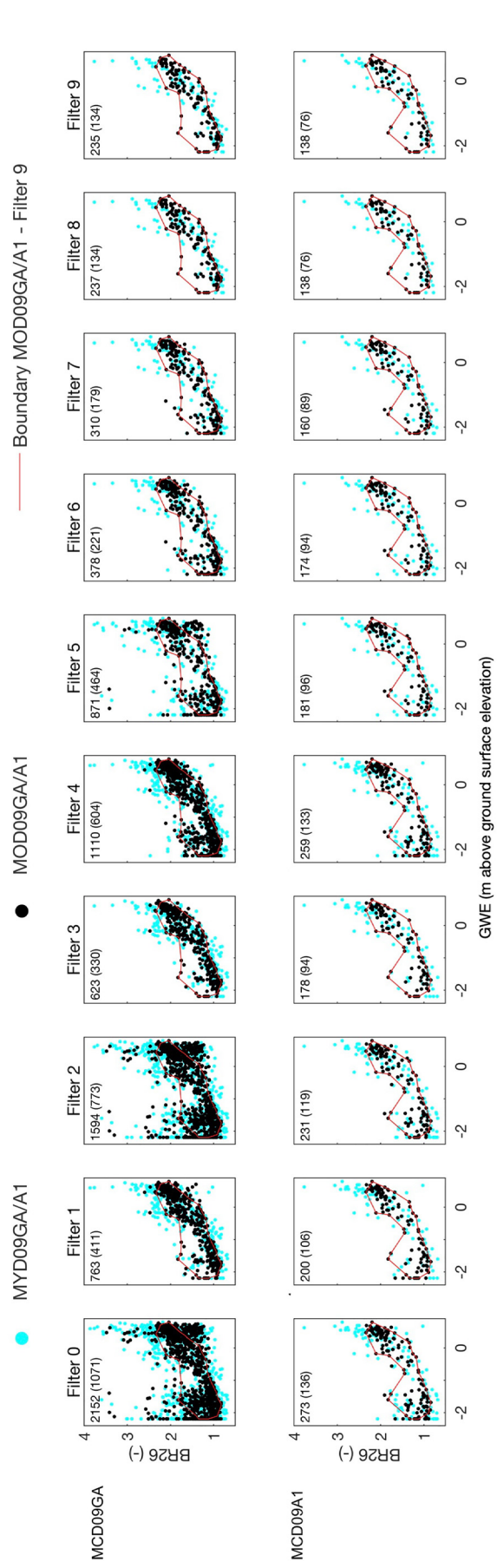

Fig. 7. BR_{26} against groundwater elevation (GWE) measured at PVWL01for alternative MODIS sensor sources, collections and filtering criteria. Red lines define the dataset boundary after application of the most constraining filter 9 on the MOD09 collection. Water level data when measured when the well was dry were excluded beforehand. Numbers in top left corners indicate the total number of points from both MOD09 and MYD09 products, and the number between brackets from MOD09 product only. (For interpretation of the references to color in this figure legend, the reader is referred to the web version of this article.)

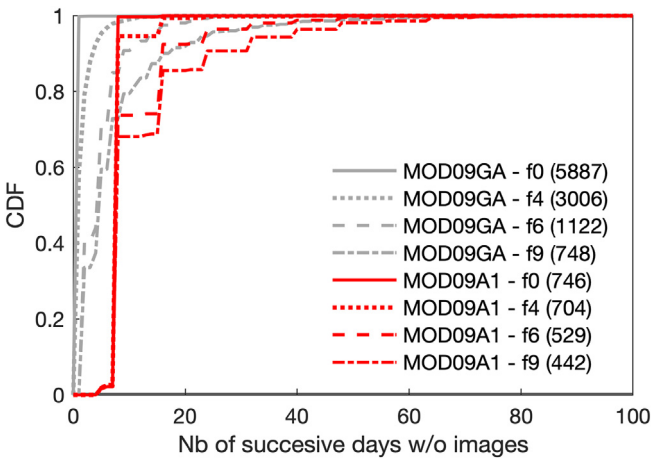

Fig. 8. Cumulative probability distribution function (CDF) of the number of successive days without image in the MOD09 product for alternative collections and filtering criteria (f#). Evaluated from FEB/2000 to MAY/2016 on data extracted from the pixel overlapping with station 1 (PVWL01). Numbers in between brackets indicate the total number of images.

Table 3
Filter combinations tested for pixel-level quality screening. The 1–4 filtering criteria certify that: (1) pixel is clear of cloud cover according to *State QA* band; (2) pixel is clear of shadow according to *State QA* band; (3) blue band reflectance is smaller than 0.1; and (4) sensor zenith angle is smaller than 32.25 degree.

Filter no.	Filtering criteria
Filter 0	None
Filter 1	1
Filter 2	2
Filter 3	1, 2
Filter 4	3
Filter 5	4
Filter 6	3, 4
Filter 7	2, 3, 4
Filter 8	1, 2, 4
Filter 9	1, 2, 3, 4

Table 4
Spectral band numbers and ranges used in MCD09 MODIS products.

Band number	Spectrum	Wavelength range (nm)
(*i* or *j* in Eqs. (1)–(2))		
1	Red	620–670
2	NIR	841–876
3	Blue	459–479
4	Green	545–565
5	SWIR1	1230–1250
6	SWIR2	1628–1652
7	SWIR3	2015–2155

water elevation, effectively an indicator of wetland moisture dynamics. In the case of Palo Verde, the WSC performed best with a single-branched tree, and the same SI was identified for both WSC and WDI. However, the SIs can be different and distinct for other applications. Importantly, a multiple-branch tree based on multiple SIs could perform best. In such a case, a multivariate regression approach would be recommended and can be readily accommodated within the proposed framework.

The wet/dry WSC that performed best for the Palo Verde case study was a single -branch decision tree with BR_{26} and a threshold at 1.66. It

Table 5
Confusion matrix to evaluate the performance of the WSC.

Monitoring station	Prediction accuracy	Kappa			Measured: Dry (GWE < −1.5 m and SWE = 0 m)	Measured: Wet (GWE > −0.2 m or SWE > 0 m)	Measured: Unknown (no SWE data and [−1.5 m < GWE < −0.2 m])
(1) PVWL01 (training data)	91.3%	0.8	Predicted	Dry	183	33	121
				Wet	7	239	21
(3) PVWL03 - PVCA07	78.0%	0.5		Dry	344	3	4
				Wet	118	84	23
(4) PVWL04 - PVCA08	90.9%	0.8		Dry	280	1	35
				Wet	36	90	51
(5) PVWL05 - PVCA08	86.8%	0.6		Dry	371	2	16
				Wet	62	53	37
(6) PVWL06 - PVCA10	88.5%	0.7		Dry	231	0	19
				Wet	39	70	138
(2) PVWL02 - PVCA11	57.1%	0.1		Dry	4	41	292
				Wet	1	52	145
All	85.3%	0.7		Dry	1413	80	487
				Wet	263	588	415
All without station 2	86.6%	0.7		Dry	1409	39	195
				Wet	262	536	270

gave good results in predicting Palo Verde wetland hydric status (87.9% correct predictions overall; kappa coefficient of 0.7). The spectral index with the highest Pearson correlation coefficient, when regressed against the water level values was NDI_{26} (R^2 = 0.71). However, BR_{26} had nearly equivalent performance (R^2 = 0.70, Supplementary Material A – Fig. A14). Correlation between the two SIs was also high (Pearson's coefficient = 0.99, see Supplementary Material A – Table A2). Thus, either could be used as a WDI for the Palo Verde wetland complex. Five other SIs had a coefficient of determination higher than 0.50: NDI_{27} (R^2 = 0.64), NDI_{25} (R^2 = 0.54), BR_{25} (R^2 = 0.54), NDVI (R^2 = 0.50) and TVI (R^2 = 0.50). NDI_{25} is identical to the NDWI proposed by Gao (1996). This index and variations of this index, produced by

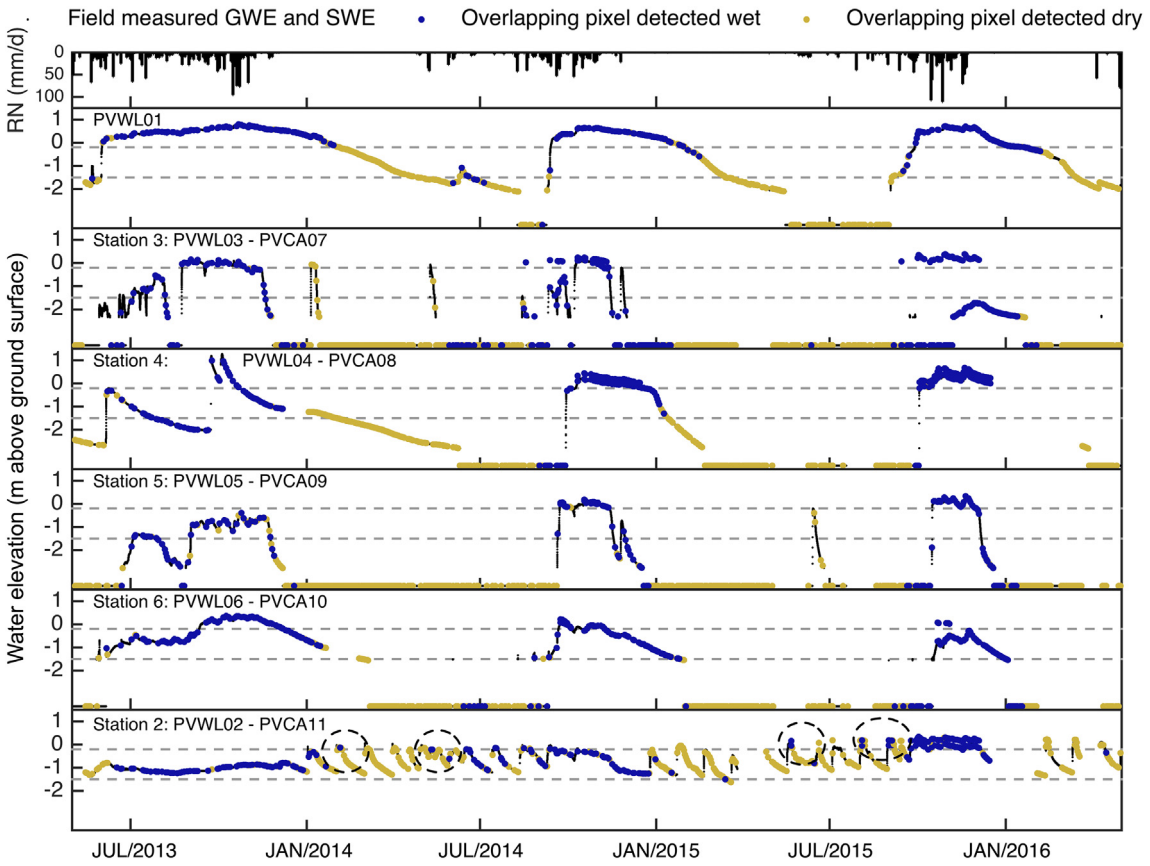

Fig. 9. Rainfall (RN), groundwater elevation (GWE) and surface water elevation (SWE), color-coded with wet/dry status as detected by the WSC. For clarity, SWE is plotted only when water was above the ground level. Dots in the bottom axis indicate when the water level fell under the sensor tip. Dashed lines correspond to the 1.5 to 0.2 m water table depth interval for which the corresponding surface hydric status is uncertain due to capillary fringe effect. Dashed circles highlight cases of river flooding events detected with the WSC. (For interpretation of the references to color in this figure legend, the reader is referred to the web version of this article.)

interchanging the three bands in the SWIR spectral region (NDI_{25}, NDI_{26} and NDI_{27}), were the three best performing SIs after BR_{26}. Although Gao's NDWI (hence NDI_{25}) was initially proposed for vegetation liquid water content, its success for detecting the Palo Verde wetland upper soil layer wetness may be explained by its sensitivity to soil moisture caused by the rapid response of vegetation water content to changing soil moisture conditions, as demonstrated by Gao (1996). It is because of these properties that authors have used an identical index named the Land Surface Water Index (LSWI) in other studies (Chandrasekar et al. 2010; Xiao et al., 2005a). The relative sensitivity of NDVI and TVI that are initially designed for vegetation monitoring is attributed to the vegetation response to the soil hydric status, but, importantly, also to the fact that these SIs are known to be sensitive to background soil moisture. Note that the EVI and SAVI, vegetation indices corrected to exclude such background effects (Huete, 1988), exhibited lower performance (R^2 = 0.40 and 0.41 respectively). These results are encouraging as they exemplify that the best SI identified for the case study wetland account for more than just the vegetation response to hydric conditions, but are also representative of the hydric status at the ground level. Tasseled Cap SIs were far weaker predictors of wetland wetness status (R^2 = 0.12, 0.30 and 0.37 for TCb, TCg and TCw respectively), which contrasts with findings from Ordoyne and Friedl (2008) and Li et al. (2015), who demonstrated the success of these SIs in the Everglades National Park wetland and a shallow and saline seasonal lake and associated marshland in Southern Spain, respectively. However, the study from Li et al. (2015) demonstrated that NDI_{26} was more strongly correlated to the shallower and more vegetated lacustrine areas, which is in concordance with our results for this shallow wetland. Finally, McFeeters' (1996) NDWI and its variations ($NDI_{42,45,46,47}$), as well as the compound index DVEL failed to capture the wetness states dynamics in our study wetland. This may be due to the more heterogeneous land cover in the Palo Verde wetland in comparison to the open water area and the paddy rice fields for which these SIs were initially developed.

Overall, the WSC and WDI identified for the Palo Verde wetland complex aligns with the findings of Chandrasekar et al. (2010) who found that NDI_{26} responded faster than NDVI to moisture changes, and Xiao et al., 2005a, who successfully used NDI_{26} to detect floods in rice paddy fields. They can be viewed as a compound indicator of the overall Palo Verde wetland hydric status – including soil moisture, liquid vegetation water, and standing water.

It is important to stress that, although using the MODIS product with a multispectral WSC/WDI common to the entire wetland area gave satisfactory results for our case study, further research should test the applicability of such approach to other wetlands with different soil and vegetation cover.

6.1.4. Sensor diagnostic mismatch

High-resolution field devices, coupled with a good knowledge of the wetland, allowed us to highlight cases of diagnostic mismatch and apparent misclassifications. We showed that GWE and SWE are not always sufficient to capture the upper soil layer hydric status. Complementing the field data with soil moisture devices could address that issue in future studies. However, such devices are often more complicated to install and maintain and are not as reliable as water elevation wells, particularly in remote areas or swelling/shrinking wetland soils. Therefore, our study highlights that the accurate depiction of wetness status in complex hydrologic systems such as wetland must rely on careful analysis of multiple and complementary data sources.

6.1.5. Capturing fast-changing hydric conditions

Results showed a weak detection potential by the wet/dry WSC of river flooding events (Fig. 9, station 2), which is likely due to mixed-pixel effects. Indeed, waters from lower intensity flooding events only partially flood the 500 × 500 m pixel area. However, peaks in the continuous WDI (BR_{26}) values occurred simultaneously with river overbank flooding events (red arrows in Fig. 10, station 2), indicating that the identifier is sensitive to these flooding events. These peak values often remained below the 1.66 threshold for the wet/dry WSC, which supports our interpretation that the weak detection rate of flooding events with binary classification is due to the mixed-pixel effects. Therefore, in the case of flooding events of smaller magnitude, abrupt changes in the WDI signal may be a better indication of flooding events than its absolute value. The Videos 1 and 2 displaying daily maps provide interactive support to visualize such changes. Additionally, the daily MOD09 product-based time series and composite maps allowed to gain insight about the soil saturation and flooding start date and interannual variability (Fig. 12), information that is critical for wetland managers (Gilman 1994) given the close link with vegetation development (Murray-Hudson et al. 2015).

6.2. Reconstruction of hydroperiod history and underlying mechanisms

The MODIS-derived end-products (Fig. 10 to Fig. 12 and Supplementary Material A Figs. A15 and A16) encode information useful to characterize wetland hydroperiod, and its 2000–2016 trajectory and drivers. Seasonal dynamics were clearly captured by the WSC and WDI, in accordance with the field water level measurements (Fig. 9). Although wetland wetness progressively increases as the rainy season starts in May, the upper soil layer was not detected as "wet" until June in most locations (Figs. 11 and 12), which suggests that an appreciable amount of accumulated rainfall is needed for the wetland's upper soil layer to become saturated or flooded. This finding is supported by the high evapotranspiration rate in this area (OTS, 2016), and the wide cracks in dry soils (Stipo, 2015) permitting infiltration of the first rainfall past the upper soil layer. The high standard deviation in WDI values at the onset of the rainy season from May to August (Fig. 12) demonstrates the large degree of interannual variability of the hydroperiod in this wetland system. The products also revealed substantial differences in hydric status dynamics – and controlling factors thereof – across the wetland, and the existence of water inputs other than rainfall. These indications that external water sources are controlling the wetland hydric status was also revealed by the field water level measurements (Fig. 5). Here, we detail the most important features revealed for each sub-wetland unit:

Palo Verde sub-wetland. Fig. 11 indicates that the Palo Verde and Nicaragua sub-wetland units take the longest to draw down, whereas the other sub-wetland units are almost entirely dry shortly after the end of the rainy season. This longer drying-down period in Palo Verde is due to topography; lower elevations in that part of the wetland implies an accumulation of deeper standing water pools.

Nicaragua sub-wetland. Fig. 12 reveals that the lower dry-down rate measured at Nicaragua (Fig. 11) is due to two areas that are frequently wet year-long: a stripe crossing the Nicaragua sub-wetland unit, and its southern corner. The latter finding suggests that the Tempisque and Bebedero rivers bordering that corner are frequently feeding the wetland with water at that location. The wet stripe might be an accumulation of the water flowing from the district through the La Bocana sub-wetland. It may also originate from intermittent streams diverging from the Tempisque River.

La Bocana sub-wetland. The postulate that irrigation water might flow by the La Bocana sub-wetland is supported by the large interannual fluctuations and more erratic hydroperiod dynamics in this site (Figs. 11 and 12), suggesting that the surface soil wetness is controlled by irrigation cycles, in addition to climate.

Poza Verde and Piedra Blanca sub-wetlands. Composite maps in Fig. 12 and Supplementary Material A – Fig. A6 showed that part of Poza Verde and Piedra Blanca sub-wetlands also maintain higher moisture levels throughout the year, which is probably due to lateral seepage, intermittent streams entering the sub-wetland, and riverbank over-flow from the Tempisque River. The strong interannual variability (large standard variation) in Poza Verde revealed in Fig. 12 might be

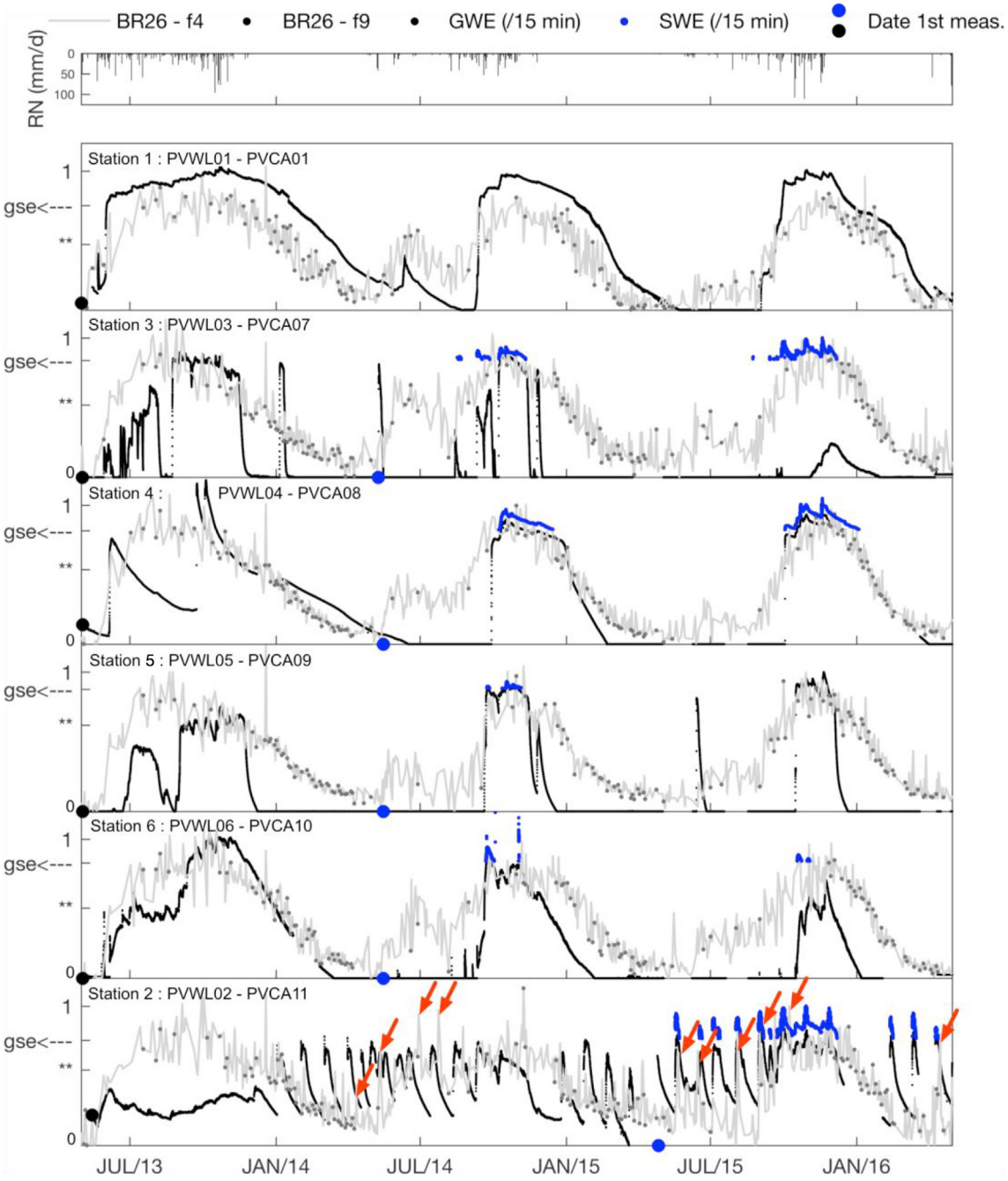

Fig. 10. Comparison of normalized surface water elevation (SWE), and groundwater elevation (GWE) with the normalized BR_{26}. SWE is only plotted when water was above the ground level. (**) and *gse* in the y-axis indicate the normalized threshold value of BR_{26} for wet/dry prediction, and ground surface elevation, respectively. Red arrows point to BR_{26}'s response to river overbank flow flooding events. (For interpretation of the references to color in this figure legend, the reader is referred to the web version of this article.)

another indication that runoff water is entering the wetland from the adjacent irrigation district.

In addition to modifying the hydroperiod locally, the pieces of evidence of influence from the irrigation district suggest that agrochemicals may periodically enter the wetland. The major influence of the surrounding rivers is also notable, especially since the discharge and dynamics of the two rivers are known to have changed drastically after the development of the inter-basin water transfer for hydropower generation and irrigation in the late 1970s (Fig. 1). Therefore, it is likely that agricultural tailwaters and the surrounding rivers may have changed the timing, volume, and quality of water entering the wetland. These lines of evidence should serve as guidance for additional monitoring and model development to better quantify and understand the nature, importance, and impacts of these external factors. These findings highlight the need to define management strategies that expand beyond the boundaries of the wetland by fully considering temporally and spatially remote hydrological connections, and the impacts of the watershed management (hydropower generation, irrigation and urban supply, return flows and canalization, land use, etc.) on the nature and dynamics of these connections.

Overall, our framework gave encouraging results illustrating that long-term wetland hydroperiod can be monitored at high-temporal and medium-spatial resolution at low cost and relatively low time investment. Besides providing data useful for model design and calibration, it

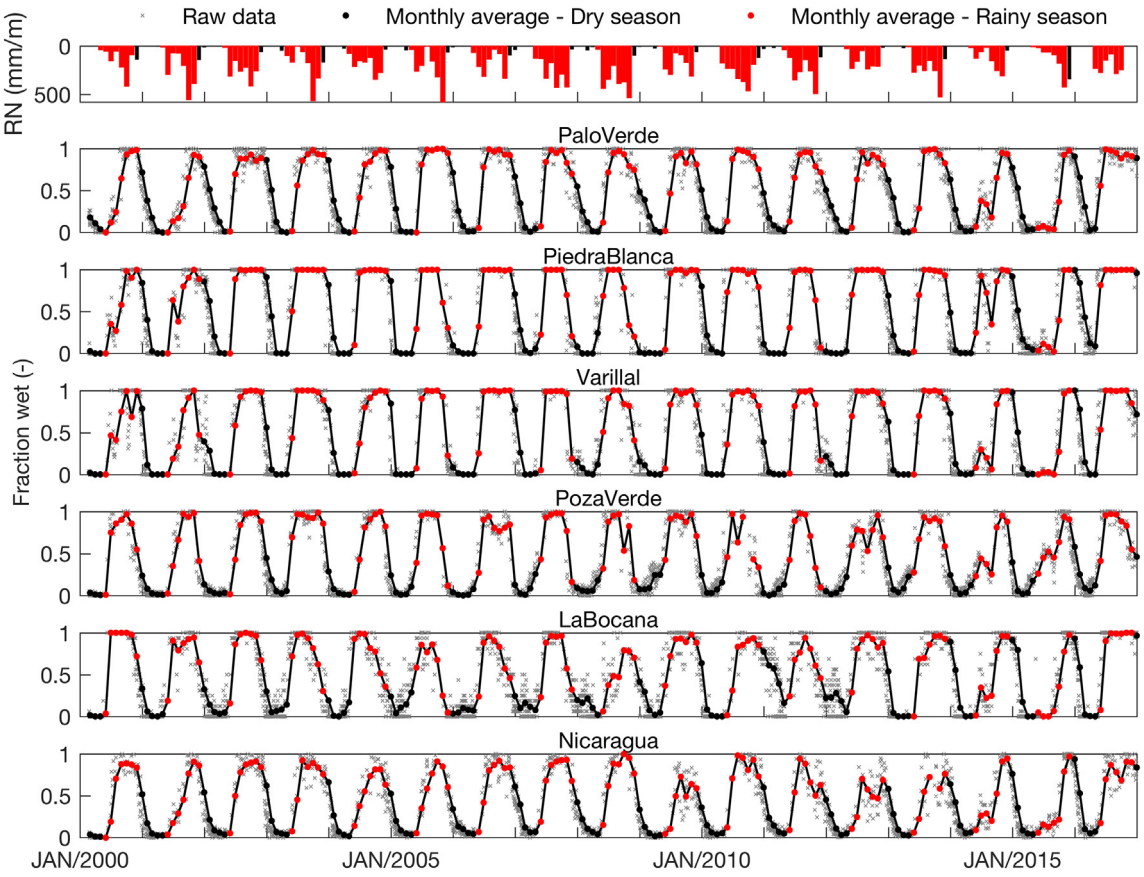

Fig. 11. Time series of the wetland areal fraction reconstructed for each sub-wetland unit.

allows to effectively reveal long-term trends and short-term transformations of wetland hydrology. Importantly, such data can fuel important information base to track and assess the path of restored wetlands (Acreman et al., 2007; Zedler 2000).

6.3. Limitations

One limitation of our approach arises from the uncertainty about the exact height of the soil capillary fringe and the degree of soil saturation as a function of groundwater elevation and evapotranspiration demand, and the overall sensor diagnostic mismatch. Future research could address this by using the proposed methodological framework with in situ soil moisture measurements in addition to water elevation. However, soil moisture sensors also come with caveats as mentioned in Section 6.1.4.

Another limitation is the coarse pixel size of the MODIS products that inevitably leads to prediction inaccuracies. Our framework with MODIS also failed in consistently detecting fast-changing processes, which we attributed to mixed pixel effects and other confounding factors. Using MODIS, a more quantitative characterization of flooding characteristics could be achieved by using more sophisticated techniques such as spectral unmixing (Halabisky et al. 2016) or multi-satellite approaches, e.g., by coupling MODIS with SAR (Aires et al. 2013; Martinis et al. 2013). On the other hand, improved prediction accuracy could be reached by using satellite products with greater spatial details such as Landsat (Collins et al. 2014; Gómez-Rodríguez et al. 2010; Halabisky et al. 2016; Huang et al. 2014). For our framework, we chose MODIS (1999-present, 500 m pixel size) over Landsat (1984-present, 30 m pixel size) products because of the lower revisit frequency of the latter (once per 16 days). Indeed, the temporal resolution of cloud-free Landsat images is insufficient to capture seasonal and fast changing dynamics in often-overcast tropical area such as in the Palo Verde National Park (Alonso et al. 2016). However, newer sensors exist that would warrant further investigation. For example, the multispectral data from the Sentinel-2 satellites launched in 2015 and 2017 (2–3 days revisit time), spatial resolution in VIS and NIR ranging from 10 to 20 m (Drusch et al. 2012; Gatti et al. 2018) should constitute an alternative once the data record is sufficiently long to document interannual dynamics. RapidEye constellation data (2009-present, daily revisit, 5 m size pixels; Tyc et al. 2005) represent another appealing option, although they do not include records in the SWIR, and their access and processing is less straightforward. Notwithstanding these alternatives, the MODIS archive remains unique for the historical information it encodes.

Another important limitation for our case study is linked to the period covered by MODIS (2000-present), which implies that the period in the 1970s during which major transformations were implemented in the Tempisque watershed (Fig. 1) remains undocumented. Therefore, the time series reconstructed in this study do not capture the transition of the system from its “pre-dam” status. However, studies have shown that the entire watershed and wetland have been witnessing a greening phenomenon (Alonso et al. 2016) and continuous land-use and cover transformation during the last decades (Convertino et al. 2016; Murcia et al. 2016). Hence, the new data can support understanding the driving processes and assess the variability, changes and trajectory of the system's “post-dam” status.

7. Conclusion

We proposed a cost-effective, straightforward methodological framework that uses the full range of publicly available MODIS Land Reflectance Products, together with fine temporal scale and high precision water elevation data, to identify and assess a site-specific spectral algorithm capable of capturing wetland hydric status. We used the

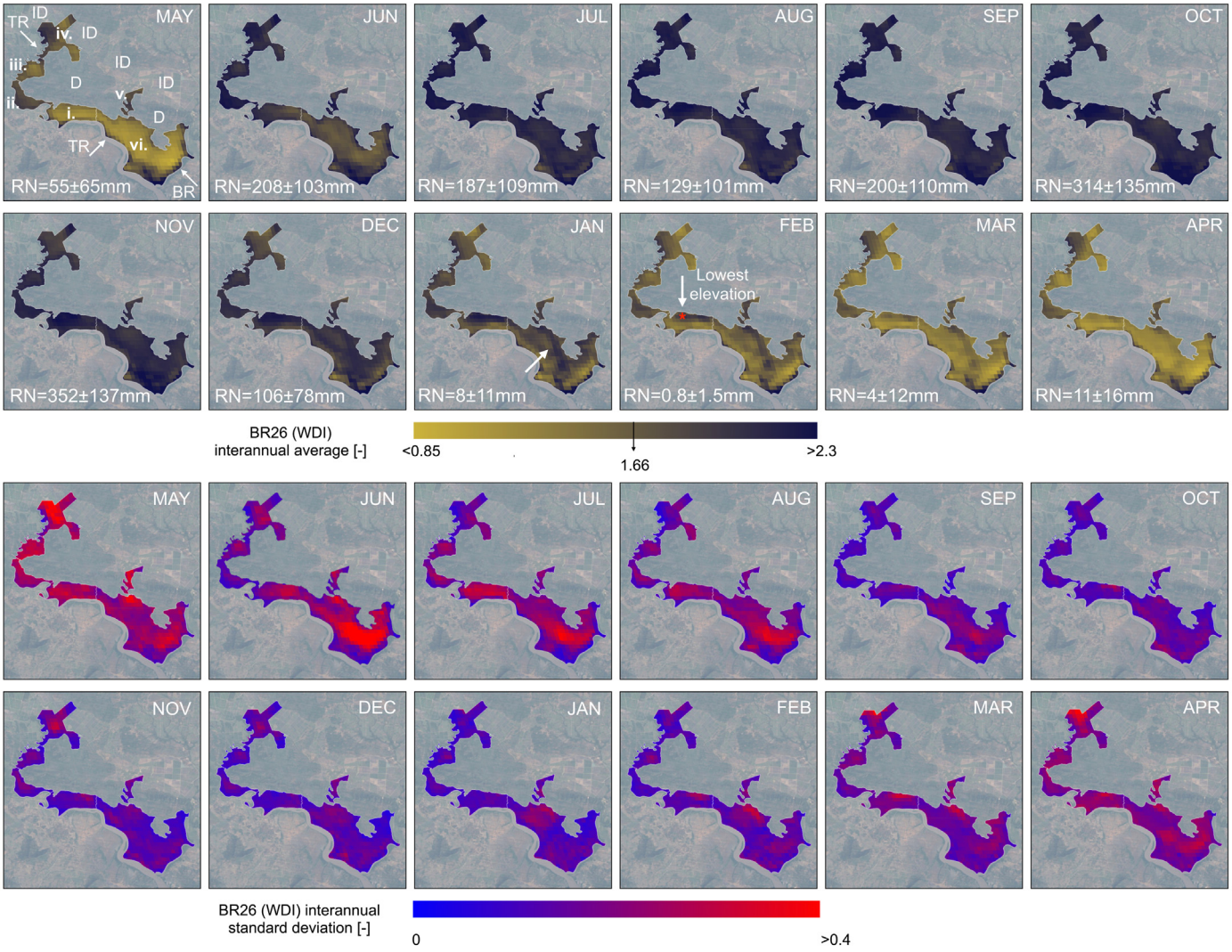

Fig. 12. Composite maps of interannual average and standard deviation of monthly averaged BR_{26} values as a proxy for wetland wetness status. The first three letters of the months are indicated in top right corners. Text in the bottom left corners is monthly rainfall (average and standard deviation). TR: Tempisque river; BR: Bebedero river; ID: irrigation district; DF: dry forest; Sub-wetlands: i: Palo Verde; ii: Piedra Blanca; iii: Varillal; iv: Poza Verde; v: Bocana; vi: Nicaragua.

method to map hydroperiod in the Palo Verde wetland in Costa Rica from 2000 to the present at a sub-weekly temporal resolution, providing new insights about its hydrology that can help guide future studies and support wetland management.

The strengths and weaknesses of our framework lie in its simplicity. It can be readily implemented for any mid-to-large scale wetlands conditioned by the availability of field-measured water elevation data. It supports characterization of intra and interannual variability and long-term trends in hydroperiod's and can shed light on underlying hydrological processes and controlling factors. Although our framework is capable of revealing the main characteristics of wetland hydroperiod and its drivers, the simplicity of the approach, combined with the coarse scale of MODIS product hamper a consistent detection of rapidly changing events and leads to some diagnostic inaccuracies.

Despite these limitations and conditioned by the availability of field-measured water level data, the proposed WSC/WDI framework remains an attractive option to help scientists and wetland managers and practitioners to readily produce new data and knowledge about the long-term spatiotemporal hydrology of any mid to large scale wetland system globally. Such data and information are instrumental for change detection and impact assessment, for model calibration and validation, and to eventually support the definition of wetland management and restoration strategies.

Supplementary data to this article can be found online at https://doi.org/10.1016/j.rse.2020.111807.

Funding

R.M.C. acknowledges the support of the Florida Water Institute Faculty Fellowship. This work was supported in part by NSF Project [Grant number CNIC OISE-1132840] and USDA NIFA Hatch Project [Grant number 1011481].

CRediT authorship contribution statement

Alice Alonso: Conceptualization, Methodology, Investigation, Software, Formal analysis, Data curation, Writing - original draft, Writing - review & editing, Visualization. **Rafael Muñoz-Carpena:** Conceptualization, Methodology, Supervision, Writing - review & editing. **David Kaplan:** Writing - review & editing.

Declaration of competing interest

The authors declare that they have no known competing financial interests or personal relationships that could have appeared to influence the work reported in this paper.

Acknowledgments

R.M.C. acknowledges the support of the Florida Water Institute Faculty Fellowship. This work is supported in part by NSF Project No. CNIC OISE-1132840 and USDA NIFA Hatch Project 1011481. The authors acknowledge Organization for Tropical Studies, and in particular Dr. Mahmood Sasa, Lic. Juan Serrano, and Dr. Carolina Murcia for their exceptional support in the design, installation and maintenance of the field instrumentation network. The authors also acknowledge Prof. Mathieu Javaux (UCLouvain, Belgium) for his constructive suggestions during the early stage of this study, Natalie Nelson (UF, USA) for the thorough editing of the document, and the Google Earth Engine team and users for their support through the user's forum. The authors acknowledge the four anonymous reviewers and the RSE editorial team for their constructive comments that allowed for significant improvements of this manuscript.

References

Acharya, S., Kaplan, D.A., Jawitz, J.W., Cohen, M.J., 2017. Doing ecohydrology backward: inferring wetland flow and hydroperiod from landscape patterns. Water Resour. Res. 53 (7), 5742–5755.

Acreman, M.C., Fisher, J., Stratford, C.J., Mould, D.J., Mountford, J.O., 2007. Hydrological science and wetland restoration: some case studies from Europe. Hydrol. Earth Syst. Sci. 11 (1), 158–169. https://doi.org/10.5194/hess-11-158-2007.

Aires, F., Papa, F., Prigent, C., 2013. A long-term, high-resolution wetland dataset over the Amazon Basin, downscaled from a multiwavelength retrieval using SAR data. J. Hydrometeorol. 14 (2), 594–607. https://doi.org/10.1175/JHM-D-12-093.1.

Aires, F., Miolane, L., Prigent, C., Pham, B., Fluet-Chouinard, E., Lehner, B., Papa, F., 2017. A global dynamic long-term inundation extent dataset at high spatial resolution derived through downscaling of satellite observations. J. Hydrometeorol. 18 (5), 1305–1325. https://doi.org/10.1175/JHM-D-16-0155.1.

Aires, F., Prigent, C., Fluet-Chouinard, E., Yamazaki, D., Papa, F., Lehner, B., 2018. Comparison of visible and multi-satellite global inundation datasets at high-spatial resolution. Remote Sens. Environ. 427–441. https://doi.org/10.1016/j.rse.2018.06.015.

Alonso, A., Muñoz-Carpena, R., Kennedy, R.E., Murcia, C., 2016. Wetland landscape spatio-temporal degradation dynamics using the new Google Earth Engine cloud-based platform: opportunities for non-specialists in remote sensing. Trans. ASABE 59 (5), 1331–1342.

Beeri, O., Phililips, R.L., 2007. Tracking palustrine water seasonal and annual variability in agricultural wetland landscapes using Landsat from 1997 to 2005. Glob. Chang. Biol., 07011911231500. https://doi.org/10.1111/j.1365-2486.2006.01306.x.

Benger, S.N., 2007. Remote sensing of ecological responses to changes in the hydrological cycles of the tonle sap, Cambodia. In: International Geoscience and Remote Sensing Symposium (IGARSS), pp. 5028–5031. https://doi.org/10.1109/IGARSS.2007.4423991.

Boers, A.M., Zedler, J.B., Drive, L., 2008. Stabilized water levels and typha invasiveness. 28 (3), 676–685.

Breiman, L., Friedman, J.H., Jerome, H., Olshen, R.A., Stone, C.J., 1984. Classification and Regression Trees.

Brisco, B., Ahern, F., Murnaghan, K., White, L., Canisus, F., Lancaster, P., 2017. Seasonal change in wetland coherence as an aid to wetland monitoring. Remote Sens. 9 (2), 158. https://doi.org/10.3390/rs9020158.

Campbell, D., Keddy, P.A., Broussard, M., McFalls-Smith, T.B., 2016. Small changes in flooding have large consequences: experimental data from ten wetland plants. Wetlands 36 (3), 457–466. https://doi.org/10.1007/s13157-016-0754-7.

Carroll, M.L., Townshend, J.R., DiMiceli, C.M., Noojipady, P., Sohlberg, R.A., 2009. A new global raster water mask at 250 m resolution. International Journal of Digital Earth 2 (4), 291–308. https://doi.org/10.1080/17538940902951401.

Chandrasekar, K., Sesha Sai, M.V.R., Roy, P.S., Dwevedi, R.S., 2010. Land surface water index (LSWI) response to rainfall and NDVI using the MODIS vegetation index product. Int. J. Remote Sens. 31 (15), 3987–4005. https://doi.org/10.1080/01431160802575653.

Collins, S.D., Heintzman, L.J., Starr, S.M., Wright, C.K., Henebry, G.M., McIntyre, N.E., 2014. Hydrological dynamics of temporary wetlands in the southern Great Plains as a function of surrounding land use. J. Arid Environ. 109, 6–14. https://doi.org/10.1016/j.jaridenv.2014.05.006.

Convertino, M., Munoz-Carpena, R., Murcia, C., 2016. "Reading the minds" for quantitative sustainability: Assessing stakeholder mental models via probabilistic text analysis. In: Public Administration and Information Technology. 20. Springer, pp. 21–38. https://doi.org/10.1007/978-3-319-25439-5_2.

Costanza, R., de Groot, R., Sutton, P., van der Ploeg, S., Anderson, S.J., Kubiszewski, I., et al., 2014. Changes in the global value of ecosystem services. Glob. Environ. Chang. 26 (1), 152–158. https://doi.org/10.1016/j.gloenvcha.2014.04.002.

Davidson, N.C., Finlayson, C.M., 2007. Earth observation for wetland inventory, assessment and monitoring. Aquat. Conserv. Mar. Freshwat. Ecosyst. 17. https://doi.org/10.1002/aqc.846.

Dixon, M.J.R., Loh, J., Davidson, N.C., Beltrame, C., Freeman, R., Walpole, M., 2016. Tracking global change in ecosystem area: the wetland extent trends index. Biol. Conserv. 193, 27–35. https://doi.org/10.1016/J.BIOCON.2015.10.023.

Domenikiotis, C., Loukas, A., Dalezios, N.R., 2003. The use of NOAA/AVHRR satellite data for monitoring and assessment of forest fires and floods. Nat. Hazards Earth Syst. Sci. 3 (1/2), 115–128. https://doi.org/10.5194/nhess-3-115-2003.

Drusch, M., Del Bello, U., Carlier, S., Colin, O., Fernandez, V., Gascon, F., et al., 2012. Sentinel-2: ESA's optical high-resolution mission for GMES operational services. Remote Sens. Environ. 120, 25–36. https://doi.org/10.1016/j.rse.2011.11.026.

Edelman, M., 1987. El distrito de riego de guanacaste (Costa Rica) y la politica del agua (the Guanacaste (Costa Rica) irrigation district and the politics of water). Anu. Estud. Centroam. 13, 95–111. https://doi.org/10.2307/25661916.

Feng, L., Hu, C., Chen, X., Cai, X., Tian, L., Gan, W., 2012. Assessment of inundation changes of Poyang Lake using MODIS observations between 2000 and 2010. Remote Sens. Environ. 121, 80–92. https://doi.org/10.1016/j.rse.2012.01.014.

Gao, B., 1996. NDWI—A normalized difference water index for remote sensing of vegetation liquid water from space. Remote Sens. Environ. 58 (3), 257–266. https://doi.org/10.1016/S0034-4257(96)00067-3.

Gatti, A., Naud, C., Castellani, C., Carriero, F., 2018. Sentinel-2 products specification document. Thales Alenia Space 1–487.

Gilman, K., 1994. Hydrology and Wetland Conservation. John Wiley & Sons, Chichester, UK.

Gómez-Rodríguez, C., Bustamante, J., Díaz-Paniagua, C., 2010. Evidence of hydroperiod shortening in a preserved system of temporary ponds. Remote Sens. 2 (6), 1439–1462. https://doi.org/10.3390/rs2061439.

Gorelick, N., Hancher, M., Dixon, M., Ilyushchenko, S., Thau, D., Moore, R., 2017. Google Earth Engine: planetary-scale geospatial analysis for everyone. Remote Sens. Environ. 202, 18–27. https://doi.org/10.1016/j.rse.2017.06.031.

Halabisky, M., Moskal, L.M., Gillespie, A., Hannam, M., 2016. Reconstructing semi-arid wetland surface water dynamics through spectral mixture analysis of a time series of Landsat satellite images (1984–2011). Remote Sens. Environ. 177, 171–183. https://doi.org/10.1016/j.rse.2016.02.040.

Hess, L., 2003. Dual-season mapping of wetland inundation and vegetation for the Central Amazon basin. Remote Sens. Environ. 87 (4), 404–428.

Huang, S., Dahal, D., Young, C., Chander, G., Liu, S., 2011. Integration of palmer drought severity index and remote sensing data to simulate wetland water surface from 1910 to 2009 in Cottonwood Lake area, North Dakota. Remote Sens. Environ. 115 (12), 3377–3389. https://doi.org/10.1016/j.rse.2011.08.002.

Huang, C., Peng, Y., Lang, M., Yeo, I.Y., McCarty, G., 2014. Wetland inundation mapping and change monitoring using Landsat and airborne LiDAR data. Remote Sens. Environ. 141, 231–242. https://doi.org/10.1016/j.rse.2013.10.020.

Huang, H., Chen, Y., Clinton, N., Wang, J., Wang, X., Liu, C., et al., 2017. Mapping major land cover dynamics in Beijing using all Landsat images in Google Earth Engine. Remote Sens. Environ. 202, 166–176. https://doi.org/10.1016/j.rse.2017.02.021.

Huete, A., 1988. A soil-adjusted vegetation index (SAVI). Remote Sens. Environ. 25 (3), 295–309. https://doi.org/10.1016/0034-4257(88)90106-X.

Jaramillo, F., Brown, I., Castellazzi, P., Espinosa, L., Guittard, A., Hong, S.H., et al., 2018. Assessment of hydrologic connectivity in an ungauged wetland with InSAR observations. Environ. Res. Lett. 13 (2). https://doi.org/10.1088/1748-9326/aa9d23.

Ji, L., Zhang, L., Wylie, B., 2009. Analysis of dynamic thresholds for the normalized difference water index. Photogramm. Eng. Remote Sens. 75 (11), 1307–1317. https://doi.org/10.14358/PERS.75.11.1307.

Jiménez, R., A, J., González, J.E., Mateo-Vega, J., 2001. Perspectives for the Integrated Management of the Tempisque River Basin.

Johnston, R.M., Barson, M.M., 1993. Remote sensing of Australian wetlands: an evaluation of Landsat TM data for inventory and classification. Aust. J. Mar. Freshwat. Res. 44, 235–252.

Jones, J., 2015. Efficient wetland surface water detection and monitoring via Landsat: comparison with in situ data from the Everglades depth estimation network. Remote Sens. 7 (9), 12503–12538. https://doi.org/10.3390/rs70912503.

Junk, W.J., An, S., Finlayson, C.M., Gopal, B., Květ, J., Mitchell, S.A., et al., 2013. Current state of knowledge regarding the world's wetlands and their future under global climate change: a synthesis. Aquat. Sci. 75 (1), 151–167. https://doi.org/10.1007/s00027-012-0278-z.

Kasischke, E.S., Melack, J.M., Dobson, M.C., 1997. The use of imaging radars for ecological applications - a review. Remote Sens. Environ. 59 (2), 141–156.

Kim, J.-W., Lu, Z., Gutenberg, L., Zhu, Z., 2017. Characterizing hydrologic changes of the great dismal swamp using SAR/InSAR. Remote Sens. Environ. 198, 1–16.

Landmann, T., Schramm, M., Colditz, R.R., Dietz, A., Dech, S., 2002. Remote sensing wide area wetland mapping in semi-arid Africa using 250-meter MODIS metrics and topographic variables. Remote Sens. 2 (7), 1751–1766. https://doi.org/10.3390/rs2071751.

Lee, Z., Weidemann, A., Kindle, J., Arnone, R., Carder, K.L., Davis, C., 2007. Euphotic zone depth: its derivation and implication to ocean-color remote sensing. J. Geophys. Res. 112 (C3), 1511–1526.

Lee, H., Yuan, T., Jung, H.C., Beighley, E., 2015. Mapping wetland water depths over the Central Congo Basin using PALSAR ScanSAR, Envisat altimetry, and MODIS VCF data. Remote Sens. Environ. 159, 70–79. https://doi.org/10.1016/j.rse.2014.11.030.

Li, L., Vrieling, A., Skidmore, A., Wang, T., Muñoz, A.-R., Turak, E., 2015. Evaluation of MODIS Spectral Indices for Monitoring Hydrological Dynamics of a Small, Seasonally-Flooded Wetland in Southern Spain. https://doi.org/10.1007/s13157-015-0676-9.

Lunetta, R.S., Knight, J.F., Ediriwickrema, J., Lyon, J.G., Worthy, L.D., 2006. Land-cover change detection using multi-temporal MODIS NDVI data. Remote Sens. Environ. 105 (2), 142–154. https://doi.org/10.1016/J.RSE.2006.06.018.

Marble, A.D., 1992. A Guide to Wetland Functional Design. CRC Press, Boca Raton, FL - USA.

Martinis, S., Twele, A., Strobl, C., Kersten, J., Stein, E., 2013. A multi-scale flood

monitoring system based on fully automatic MODIS and terraSAR-X processing chains. Remote Sens. 5 (11), 5598–5619. https://doi.org/10.3390/rs5115598.
McCarthy, T.S., Franey, N.J., Ellery, W.N., Ellery, K., 2001. The use of SPOT imagery in the study of environmental processes of the Okavango Delta, Botswana. S. Afr. J. Sci. 89, 432–436.
McFeeters, S.K., 1996. The use of the normalized difference water index (NDWI) in the delineation of open water features. Int. J. Remote Sens. 17 (7), 1425–1432. https://doi.org/10.1080/01431169608948714.
Midekisa, A., Holl, F., Savory, D.J., Andrade-Pacheco, R., Gething, P.W., Bennett, A., Sturrock, H.J.W., 2017. Mapping land cover change over continental Africa using Landsat and Google Earth Engine cloud computing. PLoS One 12 (9), 1–15. https://doi.org/10.1371/journal.pone.0184926.
Mitsch, W.J., Gosselink, J.G., 2007. Wetlands, 4 ed. John Wiley, Hoboken, New 798 Jersey.
Mitsch, W.J., Nahlik, A., Wolski, P., Bernal, B., Zhang, L., Ramberg, L., 2010. Tropical wetlands: seasonal hydrologic pulsing, carbon sequestration, and methane emissions. Wetl. Ecol. Manag. 18 (5), 573–586. https://doi.org/10.1007/s11273-009-9164-4.
Møller-Jensen, L., Yankson, P., 1994. Assessing the land cover change of accra using Landsat-TM data. Geografisk Tidsskrift-Danish Journal of Geography 94 (1), 21–25. https://doi.org/10.1080/00167223.1994.10649348.
Murcia, C., Muñoz-Carpena, R., Sasa, M., 2016. Modelaje integrado de cambio climático y socioeconómico en el manejo sostenible del recurso hídrico en la cuenca Arenal-Tempisque: Una propuesta multidisciplinaria. Rev. Ambientales. 43, 47–67. https://doi.org/10.15359/rca.43-1.5.
Murray-Hudson, M., Wolski, P., Cassidy, L., Brown, M.T., Thito, K., Kashe, K., Mosimanyana, E., 2014. Remote sensing-derived hydroperiod as a predictor of floodplain vegetation composition. Wetl. Ecol. Manag. 23 (4), 603–616.
Murray-Hudson, M., Wolski, P., Cassidy, L., Brown, M.T., Thito, K., Kashe, K., Mosimanyana, E., 2015. Remote sensing-derived hydroperiod as a predictor of floodplain vegetation composition. Wetl. Ecol. Manag. 23 (4), 603–616. https://doi.org/10.1007/s11273-014-9340-z.
Niemuth, N.D., Wangler, B., Reynolds, R.E., 2010. Spatial and temporal variation in wet area of wetlands in the prairie pothole region of North Dakota and South Dakota. Wetlands 30 (6), 1053–1064. https://doi.org/10.1007/s13157-010-0111-1.
Ordoyne, C., Friedl, M.A., 2008. Using MODIS data to characterize seasonal inundation patterns in the Florida Everglades. Remote Sens. Environ. 112 (11), 4107–4119. https://doi.org/10.1016/j.rse.2007.08.027.
Osland, M.J., González, E., Richardson, C.J., 2011. Coastal freshwater wetland plant community response to seasonal drought and flooding in Northwestern Costa Rica. Wetlands 31 (4), 641–652. https://doi.org/10.1007/s13157-011-0180-9.
Ozesmi, S.L., Bauer, M.E., 2002. Satellite remote sensing of wetlands. Wetl. Ecol. Manag. 10 (5), 381–402.
Papa, F., Prigent, C., Aires, F., Jimenez, C., Rossow, W.B., Matthews, E., 2010. Interannual variability of surface water extent at the global scale, 1993-2004. J. Geophys. Res. Atmos. 115 (12), 1–17. https://doi.org/10.1029/2009JD012674.
Pekel, J.-F., Cottam, A., Gorelick, N., Belward, A.S., 2016. High-resolution mapping of global surface water and its long-term changes. Nature 540 (7633), 418–422. https://doi.org/10.1038/nature20584.
Pope, K.O., Rejmankova, E., Paris, J.F., Woodruff, R., 1997. Detecting seasonal flooding cycles in marshes of the Yucatan Peninsula with SIR-C polarimetric radar imagery. Remote Sens. Environ. 59 (2), 157–166.
Rebelo, L. M., Finlayson, C. M., Strauch, A., Rosenqvist, A., Perennou, C., Tottrup, C., et al. (2018). The use of Earth Observation for wetland inventory, assessment and monitoring: An information source for the Ramsar Convention on Wetlands. Gland, Switzerland: Ramsar Convention Secretariat. Retrieved from www.ramsar.org/about/the-scientific-technical-review-panel.
Richter, B.D., Baumgartner, J.V., Powell, J., Braun, D.P., 1996. A method for assessing hydrologic alteration within ecosystems. Conserv. Biol. 10 (4), 1163–1174.
Rosenqvist, A., Finlayson, C.M., Lowry, J., Taylor, D., 2007. The potential of long-wavelength satellite-borne radar to support implementation of the Ramsar Wetlands Convention. Aquat. Conserv. Mar. Freshwat. Ecosyst. 17 (3), 229–244.
Sakamoto, T., Yokozawa, M., Toritani, H., Shibayama, M., Ishitsuka, N., Ohno, H., 2005. A crop phenology detection method using time-series MODIS data. Remote Sens. Environ. 96 (3–4), 366–374. https://doi.org/10.1016/j.rse.2005.03.008.
Sasa, M., Armengol, X., Bonilla, F., Mesquita-Joanes, F., Piculo, R., Rojo, C., 2015. Seasonal wetlands in the Pacific coast of Costa Rica and Nicaragua: physical and environmental characterization. Limnetica 34.
Schumann, A.W., Muñoz-Carpena, R., 2002. A simple, self-contained canal stage recorder. Appl. Eng. Agric. 18 (6), 691–696.
Spiers, A.G., Finlayson, C.M., Colin M., & Australia, Supervising Scientist, 1999. Global Review of Wetland Resources and Priorities for Wetland Inventory. Supervising Scientist.
Stipo, N., 2015. Characterization and Modeling of Water Infiltration in a Swelling Soil in the Palo Verde National Park, Costa Rica. Université catholique de Louvain, Belgium.
The Mathwork Inc, 2018. The Mathwork. Natick. United States, Massachusetts.
Trama, F.A., Rizo-Patrón, F.L., Kumar, A., González, E., Somma, D., Mccoy Colton, M.B., 2009. Wetland cover types and plant community changes in response to cattail-control activities in the Palo Verde marsh, Costa Rica. Ecol. Restor. 27 (3), 278–289. https://doi.org/10.3368/er.27.3.278.
Tsyganskaya, V., Martinis, S., Marzahn, P., Ludwig, R., 2018. SAR-based detection of flooded vegetation {\textendash} a review of characteristics and approaches. Int. J. Remote Sens. 39 (8), 2255–2293.
Tulbure, M.G., Broich, M., Stehman, S.V., Kommareddy, A., 2016. Surface water extent dynamics from three decades of seasonally continuous Landsat time series at sub-continental scale in a semi-arid region. Remote Sens. Environ. 178, 142–157. https://doi.org/10.1016/J.RSE.2016.02.034.
Tyc, G., Tulip, J., Schulten, D., Krischke, M., Oxfort, M., 2005. The RapidEye mission design. Acta Astronautica 56 (1), 213–219. https://doi.org/10.1016/j.actaastro.2004.09.029.
Vermote, E.F., Kotchenova, S.Y., Ray, J.P., 2009. MODIS Surface Reflectance user's Guide.
Waylen, P.R., Harrison, M., 2005. The coincidence of daily rainfall events in Liberia, Costa Rica and tropical cyclones in the Caribbean basin. Int. J. Climatol. 25 (12), 1665–1674. https://doi.org/10.1002/joc.1241.
Waylen, P., Laporte, M.S., 1999. Flooding and the El Nin phenomenon along the Paci ® c coast of Costa Rica. Hydrol. Process. 2638 (July 1998), 2623–2638. https://doi.org/10.1002/(SICI)1099-1085(199911)13.
Wdowinski, S., Kim, S.W., Amelung, F., Dixon, T.H., Miralles-Wilhelm, F., Sonenshein, R., 2008. Space-based detection of wetlands' surface water level changes from L-band SAR interferometry. Remote Sens. Environ. 112 (3), 681–696. https://doi.org/10.1016/j.rse.2007.06.008.
White, E., Kaplan, D., 2017. Restore or retreat? Saltwater intrusion and water management in coastal wetlands. Ecosystem Health and Sustainability 3 (1). https://doi.org/10.1002/ehs2.1258.
Wilusz, D.C., Zaitchik, B.F., Anderson, M.C., Hain, C.R., Yilmaz, M.T., Mladenova, I.E., 2017. Monthly flooded area classification using low resolution SAR imagery in the Sudd wetland from 2007 to 2011. Remote Sens. Environ. 194 (June 2007), 205–218. https://doi.org/10.1016/j.rse.2017.03.005.
Xiao, X., Boles, S., Liu, J., Zhuang, D., Frolking, S., Li, C., et al., 2005a. Mapping paddy rice agriculture in southern China using multi-temporal MODIS images. Remote Sens. Environ. 95 (4), 480–492. https://doi.org/10.1016/j.rse.2004.12.009.
Xu, H., 2006. Modification of normalised difference water index (NDWI) to enhance open water features in remotely sensed imagery. Int. J. Remote Sens. 27 (14), 3025–3033. https://doi.org/10.1080/01431160600589179.
Yamazaki, D., Trigg, M.A., Ikeshima, D., 2015. Development of a global ~ 90 m water body map using multi-temporal Landsat images. Remote Sens. Environ. 171, 337–351. https://doi.org/10.1016/J.RSE.2015.10.014.
Yan, Y.E., Ouyang, Z.T., Guo, H.Q., Jin, S.S., Zhao, B., 2010. Detecting the spatiotemporal changes of tidal flood in the estuarine wetland by using MODIS time series data. J. Hydrol. 384 (1–2), 156–163. https://doi.org/10.1016/j.jhydrol.2010.01.019.
Yuan, T., Lee, H., Jung, H.C., Aierken, A., Beighley, E., Alsdorf, D.E., et al., 2017. Absolute water storages in the Congo River floodplains from integration of InSAR and satellite radar altimetry. Remote Sens. Environ. 201 (1–16).
Zedler, J.B., 2000. Progress in wetland restoration ecology. Trends in Ecology and Evolution. https://doi.org/10.1016/S0169-5347(00)01959-5.
Zedler, J.B., Kercher, S., 2004. Causes and consequences of invasive plants in wetlands: opportunities, opportunists, and outcomes. Crit. Rev. Plant Sci. https://doi.org/10.1080/07352680490514673.
Zedler, J.B., Kercher, S., 2005. Wetland resources: status, trends, ecosystem services, and restorability. Annu. Rev. Environ. Resour. 30 (1), 39–74. https://doi.org/10.1146/annurev.energy.30.050504.144248.
Zhang, Y., Xu, H., Chen, H., Wang, F., Huai, H., 2014. Diversity of wetland plants used traditionally in China: a literature review. J. Ethnobiol. Ethnomed. 10 (1), 72. https://doi.org/10.1186/1746-4269-10-72.
Zhao, L., Yang, J., Li, P., Zhang, L., 2014. Seasonal inundation monitoring and vegetation pattern mapping of the Erguna floodplain by means of a RADARSAT-2 fully polarimetric time series. Remote Sens. Environ. 152 (C), 426–440.
Zhou, Y., Xiao, X., Qin, Y., Dong, J., Zhang, G., Kou, W., et al., 2016. Mapping paddy rice planting area in rice-wetland coexistent areas through analysis of Landsat 8 OLI and MODIS images. Int. J. Appl. Earth Obs. Geoinf. 46, 1–12. https://doi.org/10.1016/j.jag.2015.11.001.